Virtual Inertia Control Strategy for Improving Damping Performance of DC Microgrid with Negative Feedback Effect

Yang, Yaqian; Li, Chang; Xu, Jiazhu; Blaabjerg, Frede; Dragicevic, Tomislav

Published in:
I E E E Journal of Emerging and Selected Topics in Power Electronics

DOI (link to publication from Publisher):
10.1109/JESTPE.2020.2998812

Publication date:
2021

Document Version
Accepted author manuscript, peer reviewed version

Virtual Inertia Control Strategy for Improving Damping Performance of DC Microgrid with Negative Feedback Effect

Yaqian Yang, *Student Member, IEEE*, Chang Li, *Student Member, IEEE*, Jiazhu Xu, Frede Blaabjerg, *Fellow, IEEE*, Tomislav Dragicevic, *Senior Member, IEEE*

***Abstract*—Voltage of DC microgrid is prone to oscillation, originated from three factors: 1) negative damping performance of the DC converter; 2) interaction between the power converter and DC network; and 3) positive feedback of DC voltage control loop. Analogous to the relation between the force and velocity of motion, it derives the function relationship between DC current and DC voltage. Motion of DC voltage can be illustrated by the derived vectors since transfer functions between DC current and DC voltage has corresponding phase and gain at a specific frequency. It is found that it forms a positive feedback when the damping of DC converter is negative, which can destabilize DC-side voltage at the oscillated frequency. However, a negative feedback can stabilize the system and makes DC voltage attenuated. A virtual inertia (VI) control strategy is proposed for enhancement of damping performance and forming a negative feedback for the system. The proposed theoretical analysis is demonstrated by Star-Sim hardware-in-the-loop (HIL) experiments.**

***Index Terms*—oscillation, positive feedback, negative damping, virtual inertia, Star-Sim HIL experiments.**

I. Introduction

AROUSED by pressure of polluted environment and energy crisis, the renewable energies, e.g. wind and solar photovoltaics, have been increasingly utilized to meet growing energy demands and reduce greenhouse gas emissions [1]-[3]. Nowadays, as large amounts of power electronics as well as renewable energy are penetrated into power systems, power systems are gradually evolved into power electronics-dominated power systems (PEDPS). However, because of omnipresent power converters, power system is of low inertia, poor damping, and deteriorated stability, which even leads to the system oscillated [4]-[8].

Aircraft DC power systems have obtained focus in the fields of academics and engineering [9]-[15]. Refs [9], [11], [15] discuss the controller design and stability analysis of droop-controlled electrical power system for more electric aircraft. However, it does not involve in oscillation and damping of DC voltage of the system. In [10], the topology and stability analysis of DC microgrid are developed in electrified transportation systems. However, the interaction between multiple converters has not been discussed. In [12], a review of technology related to on-board microgrids is presented for the more electric aircraft. Challenge of system design is often tackled with proper load management and advanced control strategy, as highlighted in the paper. Ref. [13] proposes an adaptive backstepping approach for a DC microgrid feeding uncertain loads in more electric aircraft. Besides, the incremental negative impedance of CPLs is analyzed. A decentralized energy management strategy is proposed for energy storage unit of a more electric aircraft [14].

As clarified in the references, DC voltage is prone to oscillation because of adverse interaction between power converters and DC networks [15], and [17]-[20], or due to impedance mismatch between the output- and input-impedance [16], [21]. In Ref. [15], stability analysis is developed for a renewable energy-based DC microgrid; and a frequency-dependent virtual impedance control method is proposed for damping enhancement of DC microgrid. Eigenvalue analysis is developed to identify the impact of control parameters on stability of DC microgrid. However, once the bandwidth of the filter is determined, only the oscillation components within the bandwidth can be well filtered and dampened. But if not appropriated designed, voltage has a risk of low frequency oscillation. Moreover, the effect of the control is reliable on the system parameters.

It was reported in [17] that the impact of DC breaker system on multi-terminal VSC-HVDC system is analyzed; and dynamic interactions between multiple converters are judged by singular value analysis. Generally, constant power loads (CPL) always introduces negative damping for DC microgrid, and the dynamic behavior and stabilization of DC microgrid with CPL was analyzed in details [18]. The experimental results showed that CPL may destabilize the system, and resistive load is good for the stability of DC microgrid. Ref. [19] proposed a virtual impedance control strategy to enhance the instability of DC microgrids, originated from negative damping performance of CPL. Although the format of the control architecture is not as the same as that proposed in [15], but the physical essence is the same that the control method is to

This work was supported by the National key R&D program of China, 2018YFB0904700 and Hunan key laboratory of energy internet supply-demand and operation

The authors Y. Yang., J. Xu., and C. Li are with the College of electrical and information engineering in Hunan University, 410082, Changsha, China (e-mail: yaqianyang@hnu.edu.cn, changli@hnu.edu.cn, xujiazhu@126.com, corresponding author: Chang Li, and Jiazhu Xu)

T. Dragicevic. Author, and F. Blaabjerg are with the Department of Energy Technology, Aalborg University, Pontoppidanstræde 111, 9220 Aalborg East, Denmark (e-mail: fbl@et.aau.dk, tdr@et.aau.dk).

enhance damping for the system. However, the resistive-inductive virtual impedance cannot cover all the operation points for damping oscillation of DC voltage; besides, the selection of control parameters is restricted to the system parameters as well.

It was pointed out in Ref. [16] that the existing stabilization methods for damping oscillation even instability of the system has ignored the impacts on dynamic performance of the original cascaded system. Even in some worse cases, it would bring negative impacts for the system. Thus, it proposed an adaptive series virtual impedance control strategy to dampen instability of the system via shaping the load input impedance. Impedance-ratio criterion is utilized for the stability analysis. Ref. [20] proposed a comprehensive review for stability criteria for DC power distribution systems. Several stability criteria are discussed and compared. And the advantages and restrictions of the criteria are discussed and provide guidelines for stability investigation of future DC power systems.

Although there exist several damping control methods for enhancing stability margins of DC power systems, but it has several restrictions: 1) difficult control-tuning and reliable on system parameters; 2) may destabilize the system beyond the bandwidth if not appropriate designed; and 3) has a risk of impact on low-frequency dynamics. Hence, to improve the above shortcomings, an emulated virtual inertia control strategy is proposed for improving stability and damping oscillation of voltage in DC microgrid.

Although in [22]-[24], the emulation of virtual inertia (VI) or virtual capacitance applied in DC systems to improve transient response of the system has been reported. However, the potential capability of enhancing stability margins and damping DC-side voltage oscillation by virtual inertia control strategy has not been discussed. To fill in those blanks, this paper applies the virtual inertia control to improve the stability margin, and to mitigate oscillation of DC voltage. The contributions of this paper are as follows: 1) feedback analytical method is originally proposed to provide a novel view to observe the motion of state variables, like DC voltage; 2) a virtual inertia control strategy is proposed to mitigate oscillation of voltage; 3) different from conventional virtual inertia control technique, the proposed emulated virtual inertia control in this paper is cascaded between voltage outer-loop and current inner-loop, which does not alter the original voltage and current dual-loop control structure, thus, the robustness control structure is good; and 4) inertia and damping provided by virtual inertia control is well demonstrated by Star-Sim HIL experiments.

II. Small Signal Modeling of Aircraft DC Microgrid

In this Section, the small-signal mathematical model is developed for DC microgrid.

A. Modeling of Distributed Generation Unit-based (DGU) Converter and DC Network

DC/DC converter can behave as a virtual direct current synchronous machine (VDCSM) when applying virtual inertia control strategy aiming at the converter. Multiple distributed DC/DC converters are connected to DC-Link via DC lines, and DC-Link directly feeds power to local loads, as shown in Fig. 1.

To guarantee the reliability of DC microgrid, droop control is developed for operation of multiple DC/DC converters, as shown in Fig. 2. Clearly, DC-side capacitance is analogous to the rotor of DC machine, which is used to buffer the unbalanced powers and provide inertia support; thus, DC/DC converter behaves as a VDCSM if virtual inertia control strategy is applied, as shown in Fig. 1. Obviously, the topology of VDCSM in Fig. 1 is the same as that of DC/DC converter in Fig. 3.

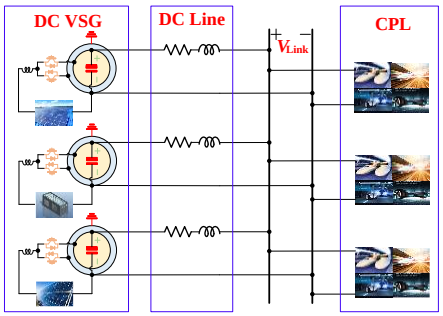

Fig. 1. The typically radial topology of DC microgrid.

It is remarkably noted that closed-loop control system of DC converter is composed of three parts: the outer-loop of voltage control, the inner-loop of current control, and pulse width modulation (PWM). To decouple the different control loops, the responses of different control loops should be set in the respective time scales. Specifically, the bandwidth of the switching frequency for PWM should be 10 times more than that of inner control loop, and the bandwidth of inner control loop should be set as 10 times as that of outer voltage loop.

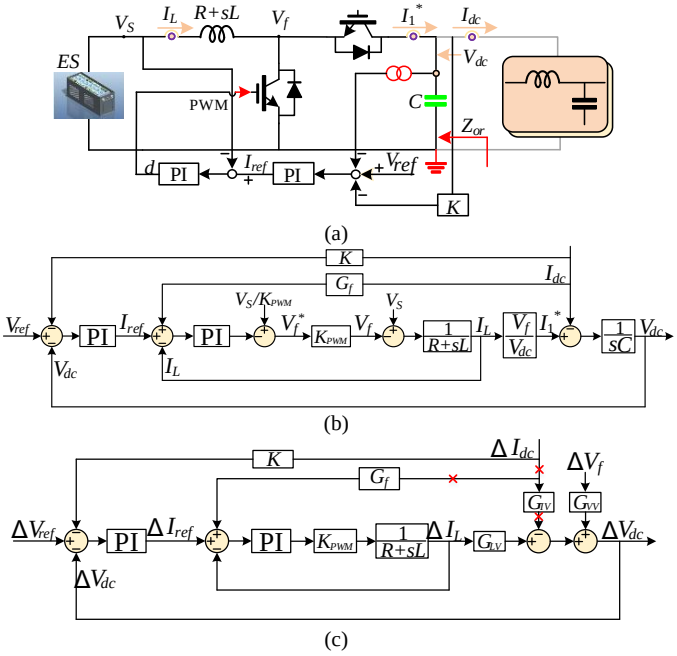

Fig. 2. Closed-loop control system of DC/DC converter-based DGU, (a) the architecture closed-loop system, (b) the closed-loop control diagram, (c) rearrangement of sub-figure(b).

Note that the physical significance of the signs in Fig. 2(b) and (c) are seen in Fig. 2(a). Especially, V_S is the DC voltage of energy storage. Because of the high frequency of sampling and switching, the time delay is not considered. The feedforward

term V_S is to eliminate the disturbance. Moreover, I_{dc} is recognized as a disturbance as for the DC/DC power converter. To avoid the adverse effect resulted from I_{dc}, here it uses the feedforward control method to enhance the anti-disturbance capability, and G_f is the feedforward term.

Thus, with rearrangement, the control diagram in Fig. 2(b) is converted into that of Fig. 2(c). Note that the red × means the control channel is disabled since that the feedforward control term has offset the impact caused by the disturbance I_{dc}.

To compromise the capability of current allocation and DC voltage deviations, the droop control gain should be better set as:

$$k_{droop} = \frac{V_{\max} - V_{\min}}{I_{rated}} \tag{1}$$

where $V_{\max}$, and $V_{\min}$ represent the allowable maximum and minimum value of DC voltage, respectively. I_{rated} means the rated current of power converter. Especially, $V_{\min}$ is limited to the linear modulation of power converter since that as for the boost converter, $V_{\min}$ should not be lower than the voltage of energy storage, i.e., V_S. Besides, to guarantee the reliable operation and lifecycle of the active (IGBT) and passive (DC-side capacitance) components, $V_{\max}$ should be confined to the nominal voltage ratings of IGBT and DC capacitance.

It is reasonable to merge multiple paralleled subsystems into one branch. Hence, all the subsystems, i.e., power converters, DC lines, and CPLs can be recognized as paralleled to the whole, as shown in Fig. 3.

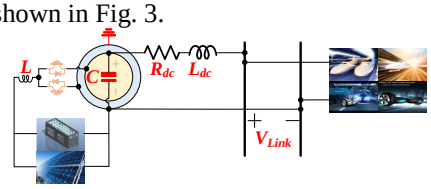

Fig. 3. Rearrangement of the topology of DC microgrid given in Fig. 2.

As shown in Fig. 2(a), inductance L is to filter the ripples of the current, and to store the energy required for boost function. The parasitic resistance contained in the inductor is always small, so, it is neglected without sacrificing the accuracy. The DC-side capacitance is to filter the ripples of DC voltage, to smooth DC voltage, and to stabilize DC voltage. According to Fig. 2(a) and Fig. 3, with the Kirchhoff voltage law (KVL) and Kirchhoff current law (KCL), we can achieve the following equations:

$$\begin{cases} V_S - V_f = L\dfrac{dI_L}{dt} + RI_L \\ I_1^* - I_{dc} = C\dfrac{dV_{dc}}{dt} \\ V_{dc} - V_{Link} = R_{dc}I_{dc} + L_{dc}\dfrac{dI_{dc}}{dt} \end{cases} \tag{2}$$

where V_S is the DC voltage of DGU; V_{Link} is the voltage of DC Link; the other quantities are given in Fig. 2(a). Further, applying Laplace transformation of the above (2) and perturbing it around the equilibrium point, it leads to:

$$\begin{cases} \Delta V_S - \Delta V_f = (R+sL)\Delta I_L \\ \Delta I_1^* - \Delta I_{dc} = sC\Delta V_{dc} \\ \Delta V_{dc} - \Delta V_{\text{Link}} = R_{dc}\Delta I_{dc} + sL_{dc}\Delta I_{dc} \end{cases} \tag{3}$$

Basing on the small signal model of the control system in Fig. 2(c), one can obtain:

$$\begin{cases} \Delta I_{ref} = (\Delta V_{ref} - \Delta V_{dc} - K\Delta I_{dc})G_V(s) \\ \Delta I_L = \Delta I_{ref}\dfrac{G_I(s)K_{PWM}/sL}{1+G_I(s)K_{PWM}/sL} = \Delta I_{ref}G_{ii}(s) \end{cases} \tag{4}$$

where K is the droop control gain; V_{ref} is the reference DC voltage; I_{ref}, I_L, and I_{dc} stand for the reference of inner-loop, the current through L, and the output current of DC converter, respectively; $G_V(s)=(k_{pv}s+k_{iv})/s$ and $G_I(s)=(k_{pi}s+k_{ii})/s$ are PI controllers of the voltage outer-loop and current inner-loop, respectively; and $G_{ii}(s)$ is the closed-loop gain of the inner-loop. Since the bandwidth of current inner-loop is high enough, that is, $K_{PWM}G_I(s)>>R+sL$. The inner-loop can be represented by the unit gain. Thus, seen from Fig. 2(c), to introduce the feedforward term to offset the impact of disturbance, i.e., ΔI_{dc}, it leads to:

$$\begin{aligned} &\Delta I_{dc}(G_f G_{LV} + G_{IV}) = 0 \\ &\Rightarrow G_f = \frac{V_{dc}}{V_f} \end{aligned} \tag{5}$$

where G_f is the feedforward term to offset the impact of disturbance brought by DC current I_{dc}.

According to the energy conservation and power balance with ignoring power losses of the converter, it leads to:

$$V_f I_L = V_{dc}I_{dc} + V_{dc}C\frac{dV_{dc}}{dt} \tag{6}$$

where C is the DC-side capacitance, which is used to smooth and stabilize the DC voltage. Perturbing the above (6) at steady point, it leads to:

$$V_{f0}\Delta I_L + I_{L0}\Delta V_f = V_{dc0}\Delta I_{dc} + I_{dc0}\Delta V_{dc} + CV_{dc0}\frac{d\Delta V_{dc}}{dt} \tag{7}$$

Clearly, from the above (7), it can be inferred that the terms, i.e., ΔI_L, ΔV_f, ΔI_{dc}, and ΔV_{dc} are interactive with each other. That is, ΔI_L, ΔV_f, and ΔI_{dc} all impose effect on the DC-side voltage. Thus, basing on the superposition principle, it can obtain the impact of ΔI_L, ΔV_f, and ΔI_{dc} on ΔV_{dc}, respectively, i.e.,

$$\begin{cases} \dfrac{\Delta V_{dc}}{\Delta I_L} = G_{LV} = \dfrac{V_f}{I_{dc}+CV_{dc}s} \\ \dfrac{\Delta V_{dc}}{\Delta V_f} = G_{VV} = \dfrac{I_L}{I_{dc}+CV_{dc}s} \\ \dfrac{\Delta V_{dc}}{\Delta I_{dc}} = G_{IV} = \dfrac{-V_{dc}}{I_{dc}+CV_{dc}s} \end{cases} \tag{8}$$

Thus, combining (2) to (8), the output impedance of the DC/DC converter can be achieved as:

$$Z_{or} = -\frac{\Delta V_{dc}}{\Delta I_{dc}} = \frac{KG_V(s)G_{ii}(s)G_{LV}(s)}{1+G_V(s)G_{ii}(s)G_{LV}(s)} \tag{9}$$

B. Constant Power Loads Modeling

The local loads are always supplied by buck power converters with dual-loop control. The local loads can be considered as a CPL, the reasons include: the response of the inner-loop controller is fast enough and much faster than that of the outer-loop controller; and resistance of local loads are

invariable; thus, when DC current is disturbed, DC voltage is almost constant and thus imposes constant power. The characteristics of constant power load are represented by:

$$p_{con} = VI \tag{10}$$

where p_{con}, V, and I represent the consumed power of CPL, the voltage across the load resistance, and the current through resistance. Then, linearizing the above (10), with ignoring the higher-order infinitesimal, it leads to:

$$\Delta V = -\frac{p_{con}}{I_0^2}\Delta I \Rightarrow \frac{\Delta V}{\Delta I} = -\frac{V_0}{I_0} = R_{CPL} \tag{11}$$

where V_0 and I_0 are the voltage and current of steady state operation points; Clearly, the port characteristic of the CPL can be represented as $-V_0/I_0$, thus, it is essentially a negative incremental resistance, which might threaten the stable operation of DC microgrid.

C. The Modeling of DC Microgrid System

Based on the modeling of parts A and B in this Section, the impedance model of the whole DC microgrid is achieved as shown in Fig. 4.

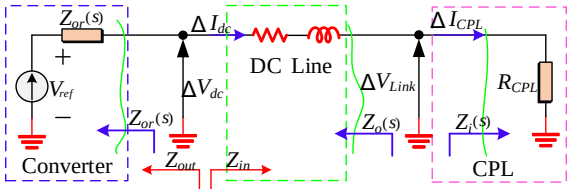

Fig. 4. The impedance model of the DC microgrid.

Fig. 4 shows the impedance model of the DC microgrid composed of the power converter, DC lines, and CPL. Especially, since that the reference V_{ref} is the desired control instruction of an active system, thus, it is reasonable to consider V_{ref} as the Thevenin's equivalent source of the system.

As can be seen in Fig. 4, Z_o and Z_i are described as follows:

$$\begin{cases} Z_o = Z_{or} + R_{dc} + sL_{dc} \\ Z_i = R_{CPL} \end{cases} \tag{12}$$

According to the minor loop gain and impedance ratio criterion given in [21], the loop gain of DC microgrid is obtained:

$$T_{loop} = Z_o / Z_i \tag{13}$$

where T_{loop} is used to evaluate the stability of the cascaded DC systems with the help of Nyquist analysis [21].

D. Current sharing mechanism between multiple power converters

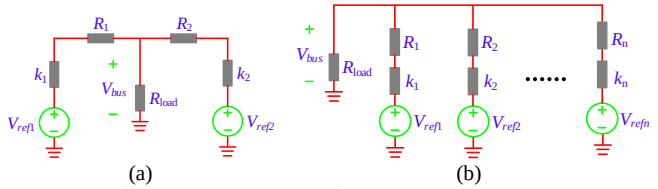

Fig. 5 Simplified equivalent circuit of DC microgrid with only considering dynamics of droop control, (a) parallel of two DC converters, (b) parallel of n DC converters.

Fig. 5 shows the simplified equivalent of DC microgrid for two cases, i.e., two paralleled converters, and n paralleled converters. Especially, two DC converters are connected to DC bus via DC lines. Actually, the DC line originally includes inductance; however, inductance neglected here for simplified model of current sharing analysis. So, we have:

$$\frac{I_{dc1}}{I_{dc2}} = \frac{R_2 + k_2}{R_1 + k_1} \tag{14}$$

It can be shown that current sharing is inversely proportional to sum of droops and line resistance.

$$\begin{cases} P_1 = V_{bus} I_{dc1} + R_1 I_{dc1}^2 \\ P_2 = V_{bus} I_{dc2} + R_2 I_{dc2}^2 \end{cases} \tag{15}$$

Substituting (14) into (15), one can obtain that:

$$\frac{P_1}{P_2} = \frac{\left[V_{bus}(R_1 + k_1) + R_1\right](R_2 + k_2)^2}{\left[V_{bus}(R_2 + k_2) + R_2\right](R_1 + k_1)^2} \tag{16}$$

Clearly, active power sharing is related with droops, resistance, and voltage.

For the generality, if n pieces of converters are connected to DC bus via DC lines, the current sharing regularity obeys that:

$$I_{dc1} : I_{dc2} : \cdots : I_{dcn} = \frac{1}{R_1 + k_1} : \frac{1}{R_2 + k_2} : \cdots : \frac{1}{R_n + k_n} \tag{17}$$

where R_n, and k_n represent line resistance and droop control of the n[th] converter, respectively. It would be noted that current sharing is inversely proportional to the sum of droops and line resistance.

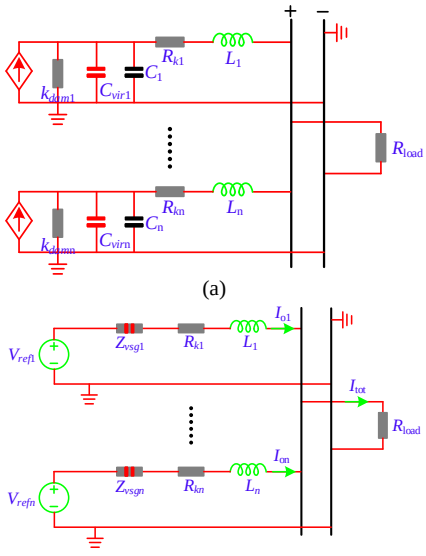

Fig. 6 Equivalent circuit for current sharing mechanism analysis with considering the proposed cascaded virtual inertia control strategy, (a) equivalent circuit with cascaded virtual inertia control, (b) rearrangement of (a)

However, the above discussion neglects the impact of virtual inertia control strategy on current sharing. In fact, the virtual inertia control is a part of the system as well, and would impact the dynamic response and dynamic current sharing.

Actually, for this cascaded virtual inertia control proposed in this paper, the output of voltage outer-loop is recognized as the input of virtual inertia control link. Thus, it can be regarded as a current-controlled source. Besides, inner-loop is much faster than other loops, thus, the impact on dynamic current sharing can be neglected here.

As shown in Fig. 6(a), cascaded virtual inertia control can contribute to adding a virtual resistance and virtual capacitance

paralleled on DC side of converter, which can be illustrated by Fig. 14. Further, the rearrangement of Fig. 6(a) can be changed into Fig. 6(b). Especially, although DC converter behaves as a controlled source, but the reference DC voltage should be regarded as the source of the system. $R_{kn}=R_n+k_n$, and $Z_{vsg}=k_{dam}//s(C+C_{vir})$.

For this regard, the current sharing law obeys that:

$$I_{dc1}:I_{dc2}:\cdots:I_{dcn}=\frac{1}{Z_{vsg1}+R_{k1}+sL_1}:\frac{1}{Z_{vsg2}+R_{k2}+sL_2}:\cdots:\frac{1}{Z_{vsgn}+R_{kn}+sL_n} \quad (18)$$

To deeply discuss the impact of cascaded virtual inertia control on current sharing of paralleled DC converters, the Bode analysis is developed. Here, we set two paralleled converters as an example to illustrate the issue. Thus, we can get the current sharing law between two converters, i.e.,

$$\begin{cases}\Delta I_{dci}=\underbrace{\dfrac{Z_{vsgj}+R_{kj}+sL_j}{Z_{vsgi}+R_{ki}+sL_i+Z_{vsgj}+R_{kj}+sL_j}}_{G_{dci}}\Delta I_{tot}\\ \Delta I_{dcj}=\underbrace{\dfrac{Z_{vsgi}+R_{ki}+sL_i}{Z_{vsgi}+R_{ki}+sL_i+Z_{vsgj}+R_{kj}+sL_j}}_{G_{dcj}}\Delta I_{tot}\end{cases}(i\neq j) \quad (19)$$

where (19) shows the law of current sharing of random two paralleled DC converters, G_{dci} and G_{dcj} represent the transfer function of current sharing, which can be used to identify the transient response in the dynamic process of current sharing.

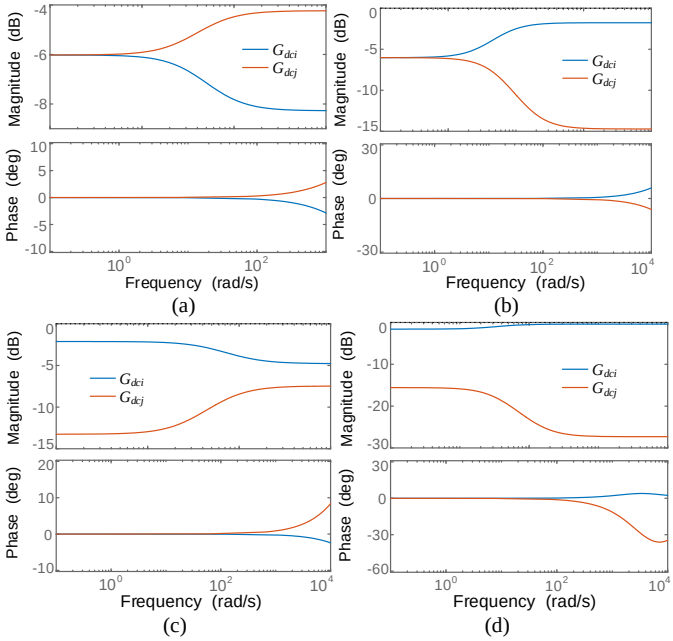

Fig. 7 Dynamic current sharing illustration, (a) different virtual inertia constant, (b) different virtual damping coefficient, (c) different droops, and (d) different droops and line length.

As for Fig. 7(a), two bode curves coincide at low-frequency regions and has a large divergence at higher-frequency region, which implies that the virtual inertia does not impact the steady state current sharing and would impose effect on transient current sharing response. Larger capacitance (red) leads to slower transient response; thus, the high frequency current response cannot be attenuated rapidly. Hence, the larger virtual capacitance results in larger current sharing in higher-frequency regions. It illustrates that too large virtual inertia constant is not good to the dynamic response in the startup (rising), because it contributes to enhance the inertia and damping for the system, especially applied in process of returning back to the equilibrium.

As for Fig. 7(b), different virtual damping coefficients are considered. Clearly, it hardly impacts the steady state current sharing but impacts the high-frequency transient current sharing. The laws has some difference to that of VSG control strategy that k_{dam} has a similar contribution to the steady current sharing like droop control. However, the architecture of proposed virtual inertia control is not the same as that of conventional VSG control. So, the laws have a little difference. Larger k_{dam} leads to smaller dynamic current sharing.

As for Fig. 7(c), the red curve corresponds to larger droop control gain. It can be inferred that larger droop gain not only results in smaller steady state current sharing but also leads to smaller dynamic current sharing.

As for Fig. 7(d), droop gain, line length of the red curve is five times larger than that of blue curve. Clearly, larger line length as well as larger droops leads to smaller dynamic current sharing; and larger droops as well as larger line resistance would lead to smaller steady state current sharing.

III. Analysis of Instability Mechanism of DC Microgrid

A. *Feedback analysis for DC voltage instability*

According to the above (9), one can obtain easily that:

$$\vec{\boldsymbol{A}}_{or}=\frac{\Delta I_{dc}}{\Delta V_{dc}}=-\frac{1+G_V(s)G_{ii}(s)G_{LV}(s)}{KG_V(s)G_{ii}(s)G_{LV}(s)} \quad (20)$$

where $\vec{\boldsymbol{A}}_{or}$ is a vector, which describes motion law of DC voltage under the effect of DC current; it also implies the impact of DC current on DC voltage.

According to Table I, the force is analogous to the current in the electric power system; while the velocity is analogous to the DC voltage across the capacitance because those are state variables. That is, based on the above (20), the inner relations between the force and velocity can be derived, which can be used to identify the motion of DC voltage with the help of vector sketch. To obtain the amplitude and phase of the vector $\vec{\boldsymbol{A}}_{or}$ at a certain frequency, the Bode diagram of $\vec{\boldsymbol{A}}_{or}$ is presented in Fig. 7.

As shown in Fig. 8, the frequency response curves of $\vec{\boldsymbol{A}}_{or}$ with changing K is presented. Clearly, the frequency region that is beyond the 1000 rad/s belongs to the negative damping region. Here we choose the three signed points, i.e., the green point, the blue one, and the red one, to develop the vector analysis, as shown in Fig. 9.

As shown in Fig. 9, the vectors are shown with the corresponding gains and phases. Absolutely, the three vectors are in the right-half plane of the circle. It is found that the horizontal component of the vector is as the same direction as that of V_{dc}, and it means that DC voltage V_{dc} can be consistently increased with the help of I_{dc}. Thus, V_{dc} cannot be stabilized and is prone to instability.

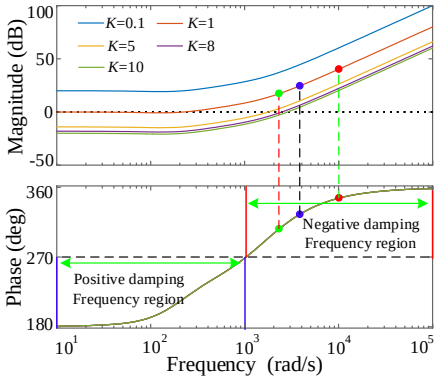

Fig. 8. Vectors diagram of $\vec{A}_{or}$ with changing droop control gain *K*.

Hence, if DC-side oscillation is triggered, the DC voltage will be divergently oscillated with the help of three vectors.

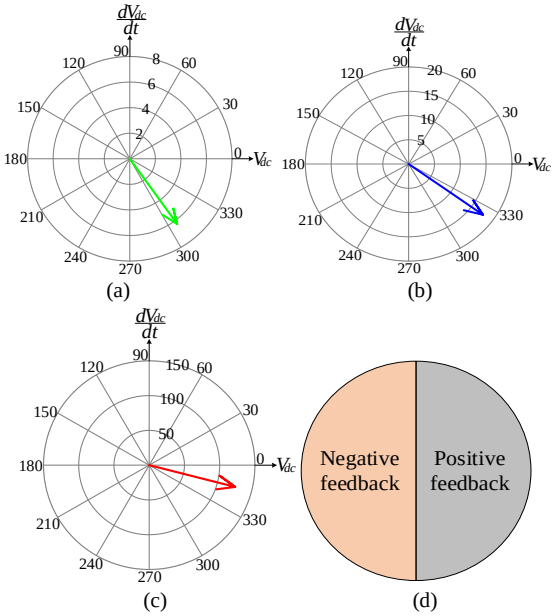

Fig. 9. Vectors of $\vec{A}_{or}$ without the virtual inertia control strategy, (a) the green point 1, (b) the blue point 2, (c) the red point 3, (d) illustration of feedback.

Before expanding the deep discussion of the DC-side stability of DC systems, we firstly give a familiar definition. As well known, according to the Newton II law, the relationship between the external force, acceleration, and velocity is acquired as:

$$\Sigma F = \mathrm{M}a = \mathrm{M}\frac{dv}{dt} \tag{21}$$

where the velocity is successively accelerated and thus leads to instability if the direction of force is the same as that of velocity.

Similarly, DC electrical system is essentially a physical system. Based on this concept, the DC-side instability can be comprehended physically, as presented in Fig. 9(a). By comparing (9) with (20), it can be inferred that $-1/Z_{or}$ is equal to $\vec{A}_{or}$, and $\vec{A}_{or}$ describes the inner relations between DC current and DC voltage. So, $\vec{A}_{or}$ can determine the motion and change of DC voltage.

The vector of $\vec{A}_{or}$ has a certain amplitude and phase at a specific frequency:

$$\vec{A}_{or} = A_{or}\angle\varphi \tag{22}$$

where A_{or} and φ are the gain and phase of the vector at a certain frequency; according to the phase and gain in Bodes of $\vec{A}_{or}$, the vector has a determined position in the vector diagram.

Fig. 10(a) shows the case of green operation point as shown in Figs. 8. In Fig. 10(a), the yellow arrow (V_{dc0}) represents the initial operation point of DC voltage; the blue arrow (V_{dc1}) is the operation point of DC voltage with the disturbance; the purple arrow is the initial DC current, i.e., I_{dc0}; and the green arrow is the DC current with the disturbance, i.e., I_{dc1}. Clearly, when a disturbance makes DC voltage increased (operation point moving from V_{dc0} to V_{dc1}), with the help of $\vec{A}_{or}$, the amplitude of DC current is increased as well. It can be seen that the direction of the horizontal component of DC current is increased as well, which is in the same-phase with that of DC voltage. Hence, it will compel the DC voltage consistently increased, and the increased voltage will further make DC current increased. Thus, it forms a positive feedback (PF), which lead to DC-side voltage is prone to instability and divergent oscillated.

Thus, the same-phase DC current absolutely charges the DC-side capacitor thus make DC voltage further increased and cannot return back to the initial static operation point or be stabilized at another steady operation point. If the DC voltage is oscillated, the waveform is inevitably divergent. Hence, it forms a PF and behaves as the characteristics of the negative damping, which is unfavorable to the stability of DC voltage.

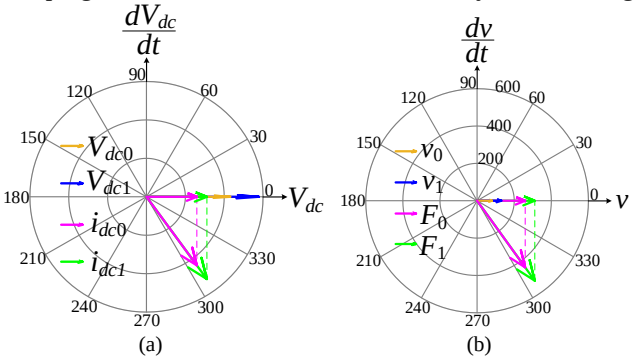

Fig. 10. Physical mechanism of DC-side instability interpreted by the motion of DC voltage and DC current, (a) vector analysis for I_{dc}-V_{dc}, (b) vector analysis for *F*-*v*.

Fig. 10(b) describes the relation between the force and the motion velocity. The force is increased as well and the direction is as the same as velocity with the help of force, when velocity is increased. Thus, it can make the physical object accelerate consistently, which forms a PF and can destabilize the velocity (according to Newton I law, the system can always remain the original motion state if not disturbed, and this belongs to the stable operation point; while the successive acceleration is undoubtedly unstable).

IV. Working Mechanism of Virtual Inertia Control Strategy

In [22]-[28], the virtual synchronous generator (VSG) control strategy is mentioned. However, few publications have fully exploited the function of the enhancement of inertia and

damping of virtual inertia control to mitigate DC-side instability of DC systems, and it is discussed in this Section.

A. Introduction of Virtual Inertia Control Strategy

As well known, the frequency oscillation occurred in SG-dominated power systems can be damped with the inertia of the rotor. With this concept, DC-side oscillation occurred in DC systems can be damped by means of emulating the external characteristics of the SG and thus enhancing the inertia of DC systems.

To emulate the motion characteristics, inertia, as well as damping performance of VSG to acquire virtual inertia for DC microgrid, the control equation of the proposed virtual inertia can be depicted as:

$$T_m - T_e - D_{dam}(\omega_{vir} - \omega_n) = \frac{1}{J_{vir}} \frac{d\omega_{vir}}{dt} \tag{23}$$

$$i = C\frac{dV_{dc}}{dt} \Leftrightarrow T_{vir} = \frac{1}{J_{vir}} \frac{d\omega_{vir}}{dt} \propto C_{vir} \frac{dV_{vir}}{dt} \tag{24}$$

From the above (24), the current in electrical systems corresponds to the driver force which can enforce the capacitor change its motion state, i.e., altering DC voltage. Actually, the current can be analogous to the force moment in (23), whose essence is alike.

TABLE I
COMPARISON AMONG PHYSICAL OBJECT, GENERATOR ROTOR, AND CAPACITOR

Items	*Physical Object*	*Generator Rotor*	*DC-side Capacitor*
Stored energy	$Mv^2/2$	$J\omega^2/2$	$CV_{dc}^2/2$
Momentum	Mv	$J\omega$	CV_{dc} (charge)
State variable	v	ω	V_{dc}
Force	Ma (F/T)	$Jd\omega/dt$	CdV_{dc}/dt (i)
Acceleration	a	$d\omega/dt$	dV_{dc}/dt
Inertia	M	J	C

B. Mechanism of Virtual Inertia Control for Improving Damping Performance

Based on the above (23), it can be concluded that when DC-side voltage is oscillated, the virtual inertia current instruction is produced to mitigate the instability; and the virtual inertia part does not function in steady state. Besides, virtual damping factor will inevitably lead to the deviation of DC voltage. In this part, it is illustrated that the virtual damping control part does not contribute to the damping of DC-side oscillations, while virtual inertia control part can supply DC systems with enough inertia and stability margins. According to (23)-(25), and (28), the small signal control system with virtual inertia control strategy is given in Fig. 11.

From (24), it can be concluded the larger virtual capacitance can produce more virtual inertia current to provide inertial support. Besides, the larger virtual inertia can lead to slower rate of change of virtual angular frequency; if C_{vir} is large enough, virtual angular frequency is stable and smooth. It would be illustrated that the virtual DC voltage is proportional to virtual angular frequency as follows, i.e., larger C_{vir} leads to smoother DC voltage and slower rate of change of frequency.

To comprehend the physical meaning of the virtual inertia control strategy, the comparison between object, rotor, and DC-side capacitor is developed in Table I. Note that, in a physical system, the mass M is recognized as the measure of inertia of physical object. And the larger mass means that the motion state of the object is not easier to be altered; that is, the acceleration is slower, and thus, the velocity v varies slower. Similarly, the same characteristic arises as for the rotor and capacitors. The larger capacitance indicates that the DC voltage changes slower. Consequently, larger virtual inertia constant suggests larger inertia or mass as for DC systems, which can decelerate the rate of change of DC voltage as well as the oscillated frequency of DC voltage.

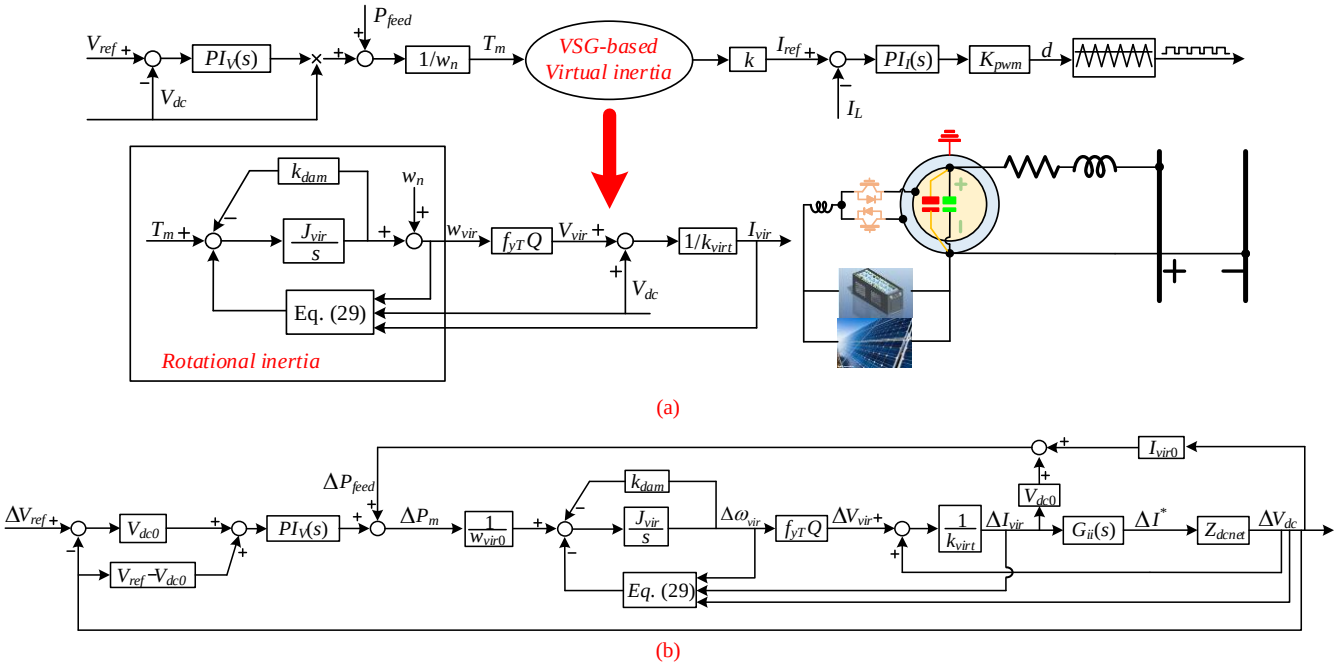

Fig. 11. Control system of DC microgrid with VI control, (a) the detailed control block and implementation of virtual inertia, (b) the samll signal model with virtual inertia control strategy.

Virtual inertia control makes DC microgrid own larger inertia and damping. Perturbing (23) around the equilibrium point leads to:

$$\Delta T_m - \Delta T_e = (D_{dam} + \frac{1}{J_{vir}} s)\Delta\omega_{vir} \quad (25)$$

From (25), it can be inferred that one virtual resistance and one virtual capacitance are emulated on DC-side of DC microgrid, which is shown in Fig. 12. Indeed, ω_{vir} is coupled with virtual DC voltage V_{vir} through $f_{yT}Q$. It should be noted that J_{vir} is justly inversely proportional to C_{vir}. So, the larger virtual inertia can lead to slower rate of change of DC voltage, since that ω_{vir} is proportional to V_{vir}. An added virtual capacitance provides larger inertia support and leads to system more robust. Active power balance equation in (7) can be rewritten as:

$$\frac{\Delta P_{dc}}{V_{dc1}^{\ 0}} - \Delta I_{dc1} = (\frac{I_{dc1}^{\ 0} + CV_{dc1}^{\ 0} s}{V_{dc1}^{\ 0}})\Delta V_{dc1} = (D_{dc} + Cs)\Delta V_{dc1} \quad (26)$$

where ΔP_{ac} means the active power; D_{dc} denotes the ratio, i.e., $I_{dc1}^{\ 0}/V_{dc1}^{\ 0}$.

Comparing (25) with (26), it can be found that two formulas resemble, which suggests that virtual inertia control can not only emulate inertia but also function to buffer active power and provide power support for DC system. Active power balance equation is essentially a virtual inertia control equation; and active power balance is maintained by DC-side capacitance; thus, it can be rigorously inferred that virtual inertia control equation is absolutely to emulate a virtual capacitance on DC-side of the system.

By comparing (25) and (26), it can be known that the rotational inertia J_{vir} is justly inversely proportional to the virtual capacitance C_{vir}. From the formula (23), it can be inferred that J_{vir} is proportional to the rate of change of DC voltage, because of $1/J_{vir} \propto \frac{dV_{vir}}{dt} \propto \frac{d\omega_{vir}}{dt}$

The potential energy stored in virtual inertia can be calculated as:

$$W_{inertia} = \frac{1}{2} C_{vir} V_{vir}^{\ 2} \quad (27)$$

Actually, the original inertia hidden in DC network is mainly dependent on total of DC capacitance, which is limited. The source, like photovoltaics (PV), winds, has little inertia to support the DC network. Although supercapacitor behaves as a capacitor; but it cannot contribute to DC network with enough inertia if a controller has not related the supercapacitor with DC network.

It can be seen from (27), the potential energy stored in virtual inertia can be provided by output of PV, energy storages, or other renewable energy. Essentially, essence of virtual inertia is to emulate the "slow inertia characteristics" to let power fluctuation less and slower as well as slower rate of change of energy. Electromagnetic power of VSG can be obtained as:

$$P_e = \omega_{vir} T_e = V_{dc} I_{vir} \quad (28)$$

where it can be seen that it is the two forms of active power; and the core idea is originated from Table I, where current is equivalent to force moment, and DC voltage corresponds to rotor angular frequency.

Perturbing the above (28), one can derive that:

$$\Delta T_e = \frac{I_{vir0}}{\omega_{vir0}} \Delta V_{dc} + \frac{V_{dc0}}{\omega_{vir0}} \Delta I_{vir} - \frac{V_{dc0} I_{vir0}}{\omega_{vir0}^{\ 2}} \Delta\omega_{vir} \quad (29)$$

By means of the above analysis, the details of virtual inertia control parts are presented in Fig. 11(a), where the virtual inertia is essentially to contribute to enhancing damping performance and inertia for the systems, thus, the core idea is to emulate the dynamics of conventional SG for acquiring inertia and damping. Virtual DC voltage is to add the damping of the system to make DC voltage change slower. As shown in topology, DC power converter can behave a virtual synchronous machine when implemented with virtual inertia control strategy. Fig. 11(b) displays the small signal model of closed-loop control system. V_{vir} is the virtual DC voltage of the proposed virtual inertia control strategy. P_{feed} is the feedback active power to improve the response speed and counterbalance the effect of disturbance, and Z_{dcnet} is the equivalent impedance seen from output port of DC power converter. k_{virt} is the virtual resistance factor.

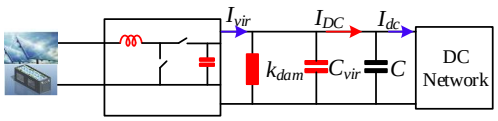

Fig. 12. Equivalent physical circuit with VI control.

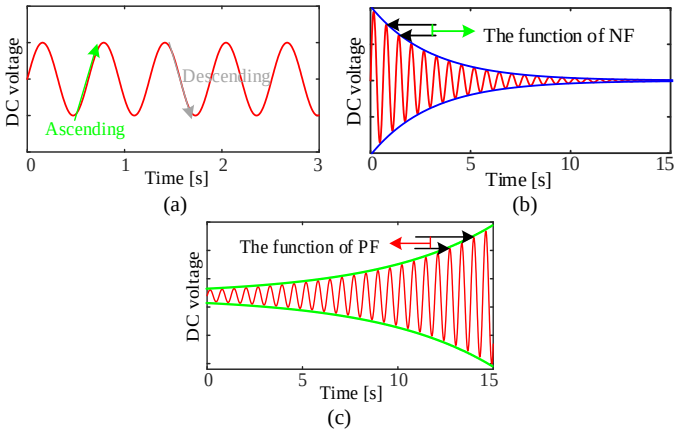

Fig. 13. The schematic of the transients interpreted by vector analysis, (a) the sketch of oscillation when subjected to a disturbance, (b) attenuated oscillation hindered by NF, (c) divergent oscillation by PF.

To further comprehend the concept of PF and NF in the case of DC-side oscillation, Fig. 13 shows the oscillated transients of the system when subjected to disturbance. As shown in Fig. 13(a), the green arrow is defined as the ascending process, and gray arrow refers to the descending process of oscillation.

Clearly, if the vector $\vec{A}_{or}$ is located in region of NF, the DC current will hinder the change of DC voltage. Negative feedback indicates that DC current is always hindering the change of DC voltage, which can stabilize the system and make DC voltage tend to be stable.

Specifically, as shown in Fig. 13(b), DC voltage is increasing in the ascending process of a certain cycle; then, it cannot reach the same level in the ascending process of the next cycle because negative feedback always contributes to hindering the change of DC voltage. Similarly, DC voltage is declined in the descending process of a certain cycle; then, it would be declined less than that of the former cycle because negative feedback functions to impede the variation of DC voltage.

Hence, DC voltage is convergent and system can operate stably. That is, negative feedback can improve damping performance of the system and make DC voltage attenuated.

However, if the vector $\vec{A}_{or}$ is located in the region of PF, DC current positively compels the change of DC voltage. It suggests that the impact of DC current on motion of DC voltage is positive. That is, in the ascending process, DC voltage will be further increased in the next cycle with the function of PF; while in the descending process, DC voltage will be further descended. As a result, DC voltage will be divergent other than convergent. In general, PF characteristic of $\vec{A}_{or}$ is always to support the change of motion of DC voltage and compels it go ahead continually. Hence, PF will destabilize DC voltage, and makes it divergent, which can be seen in Fig. 13(c).

As shown in Fig. 14, when a disturbance is imposed on DC voltage and makes it increased, with the function of $\vec{A}_{or}$, the DC current is increased, and the horizontal component is opposite to DC voltage, and thus makes it declined. Afterwards, the declined DC voltage further make DC current decreased and return back to the initial point. Hence, it forms a NF, and supplies a positive damping for DC voltage. In this case, with the function of DC current, the positive damping and NF is supplied and makes DC voltage stabilize at a steady level.

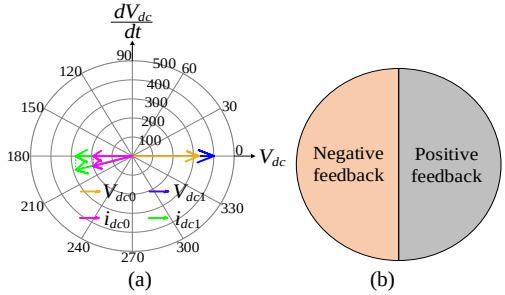

Fig. 14. The motion of DC current Δi_{dc} and DC voltage ΔV_{dc} with virtual inertia strategy, (a) vector sketch, (b) the sketch of PF and NF.

C. Robustness analysis

Before robustness analysis, we should introduce two transfer functions as well as the definitions.

Define G as the transfer function of forward channel, and K as the feedback gain in the feedback channel. Thus, control loop gain is obtained as: $L=GK$. As for a control system, sensitivity function, defined as S, and complementary sensitivity function, defined as T, are two important indexes to identify system dynamic performance, robustness, and stability. If the system wants to get a good tracking performance and anti-disturbance capability, L should be as much as possible.

For a single-input-single-output system, S and T can be obtained as:

$$\begin{cases} S = \dfrac{1}{1+L} \\ T = \dfrac{L}{1+L} \end{cases} \tag{30}$$

where it can be easily seen that we have $S+T=1$; that is, as for system performance, S is contradictory to T.

However, S and T are two frequency-dependent vectors, which have both amplitude and phase. Thus, the following inequality can be derived:

$$\big||S|-|T|\big| \le |S+T| \le |S|+|T| \tag{31}$$

Hence, it can be inferred that the absolute of difference of two functions can be below 1. But the sum of two functions has a large risk of above 1.

It is reasonable to define the peak value of S and T by means of H_∞ norm, i.e.,

$$\begin{cases} M_S = \max\limits_{\omega} |S(j\omega)| = \|S\|_\infty \\ M_T = \max\limits_{\omega} |T(j\omega)| = \|T\|_\infty \end{cases} \tag{32}$$

The premise to guarantee robustness is to satisfy nominal performance and robust stability simultaneously. As shown in Fig. 15, robust stability can be guaranteed if and only if the smaller red circle has not encircled the point (-1, 0), i.e.,

$$\begin{aligned} &\text{RS} \Leftrightarrow \ |\omega_I L| < |-1-L| \forall \omega, \\ &\left|\frac{\omega_I L}{1+L}\right| < 1, \forall \omega \ \Leftrightarrow \ |\omega_I T| < 1, \ \forall \omega \end{aligned} \tag{33}$$

where ω_I is the multiplicative uncertainty.

The nominal performance of the system can be obtained if and only if the large blue circle of which the radius is ω_p is not intersected with the open loop transfer function curve, i.e.,

$$\begin{aligned} &\text{NP} \Leftrightarrow \ |\omega_P| < |-1-L| \ \ \forall \omega, \\ &\Leftrightarrow \ |\omega_P S| < 1, \ \ \forall \omega \end{aligned} \tag{34}$$

As a result, the robustness can be guaranteed if and only if the two circles have no intersections. Thus, the robustness can be guaranteed if the following inequality is satisfied:

$$\text{RP} \Leftrightarrow \ \max_{\omega}(|\omega_P S| + |\omega_I T|) < 1 \tag{35}$$

where RS, NP, and RP represent robust stability, nominal performance, and robustness performance of the system, respectively.

Considering the multiplicative uncertainty, we let $\omega_I=\omega_p=0.5$, the robustness can be judged referring to Fig. 15(a). The robustness can be guaranteed if and only if the circle of which the center is (-1, 0) and radius is ω_p has no intersections with that the circle center is on the curve and radius is $\omega_I L$.

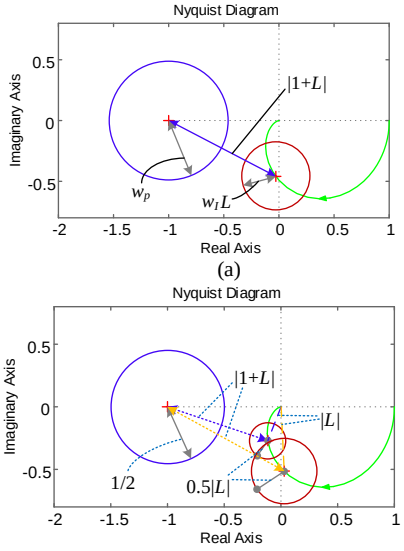

Fig. 15. Schematic diagram of S and T, (a) schematic diagram of robust stability, (b) schematic diagram of robustness performance

As shown in Fig. 15(b), the sensitivity and complementary sensitivity functions are obtained to identify the robustness of the systems. And the impact of virtual inertia as well as virtual damping on DC microgrid is discussed. Clearly, both sensitivity and complementary sensitivity have a sharp peak as shown in Fig. 16(a), i.e., $\|S\|_\infty + \|T\|_\infty > 2$, which leads to the system less robust. The robustness is poor for this case because of without the proposed virtual inertia control.

As for Fig. 16(b), (c), and (d), virtual inertia constant is increased, but both sensitivity and complementary sensitivity functions are almost unchangeable. Clearly, sensitivity of all of three cases is extremely low, indicating good robust stability. $\|S\|_\infty + \|T\|_\infty \approx 1$ is satisfied in all the frequency regions, suggesting good robustness. Besides, it can be inferred that the proposed cascaded virtual inertia control strategy is very helpful for robust stability as well as robustness since that no matter of virtual inertia constant. It illustrates that the architecture of proposed virtual inertia radically improves robustness.

As tested in Fig. 16(e) and (f), two sizes of virtual damping constant are considered. Clearly, both robust stability and robustness are super. It can be concluded that the architecture of proposed cascaded virtual inertia control is robust. And it can bring good robustness for DC system no matter of size of virtual damping.

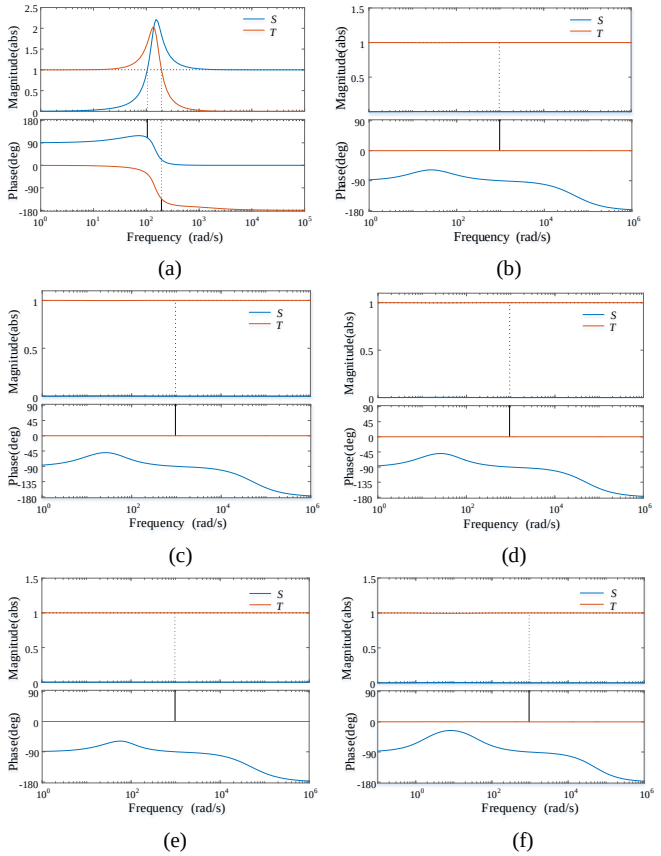

Fig. 16 The impact of virtual inertia and virtual damping on system robustness, (a) without virtual inertia and virtual damping, (b) C_{vir}=5 mF, D_{dam}=3, (c) C_{vir}=0.05 F, D_{dam}=3, (d) C_{vir}=0.5 F, D_{dam}=3, (e) C_{vir}=0.005 F, D_{dam}=0.3, (f) C_{vir}=0.005 F, D_{dam}=30

The robustness analysis is developed with considering the impact of time delay, and the results are presented in Fig. 17. Obviously can be seen, $\|S\|_\infty + \|T\|_\infty$ gets larger when time delay is increased, especially for case (c) and (d), $\|S\|_\infty + \|T\|_\infty > 2$ which indicates that the time delay is unfavorable to the robustness of the system since that two high peak of sensitivity and complementary sensitivity is not good to the robustness, and its value should have an upper bound. Hence, time delay is not beneficial for robust stability as well as robustness.

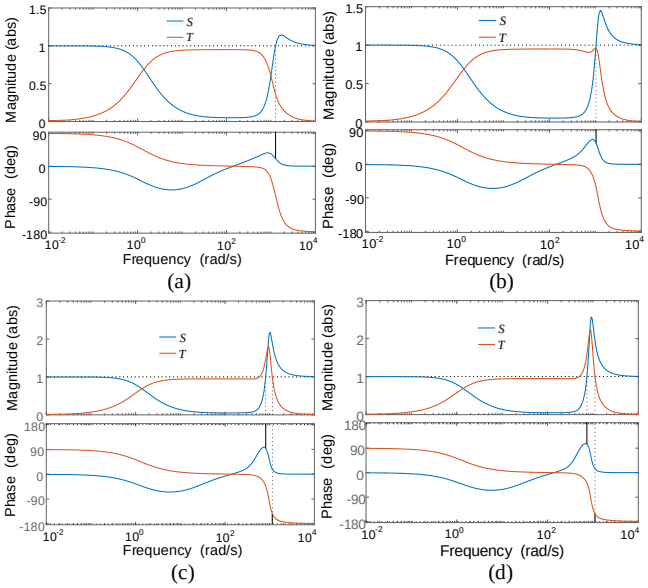

Fig. 17. Robustness performance analysis with considering time delays, (a) without time delays, (b) T_{del}=0.001 *s*, (c) T_{del}=0.005 *s*, and (d) T_{del}=0.01 *s*

D. Eigenvalue analysis

To further intuitively identify the impact of virtual inertia as well as virtual damping on stability of the studied microgrid, eigenvalue analysis is developed with altering system parameters. The red x means the poles of system; the blue o means zeros of system.

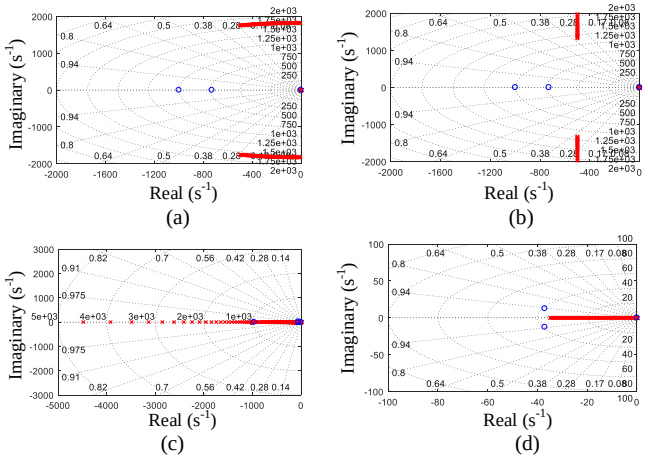

Fig. 18. Eigenvalue analysis, (a) variation of R_{line}, (b) variation of C, (c) variation of C_{vir}, (d) variation of D_{dam}

It can be found that the damping of the system is enhanced as line resistance is increased without any change of oscillation frequency, as shown in Fig. 18(a). Fig. 18(b) shows the eigenvalue movements as capacitance changed. As can be clearly seen that oscillation frequency is declined as well as damping performance enhanced as DC capacitance is enlarged.

It can be inferred that DC capacitance not only alter the oscillated frequency of dominant eigenvalue, but also change the damping.

Fig. 18(c) and (d) depict eigenvalues when virtual inertia and virtual damping is changed, respectively. It shows that the dominant eigenvalues are located in the negative real axis, which indicates that the damping of the system is enough, which means that the proposed cascaded virtual inertia control strategy can improve the damping performance of the system. Besides, both Fig. 18(c) and (d) shows that eigenvalues moves along with the negative real axis, which suggests that once the cascaded virtual inertia control is introduced, the damping performance of the system is significantly enlarged and improved no matter of the size of virtual damping or virtual inertia. Very similar with the law of robustness analysis, it fully explains that the proposed cascaded virtual inertia control can radically enhance the damping performance, and mitigate oscillation.

E. Sensitivity analysis and control parameters tuning

According to the circuit- and control-equations, the small-perturbation state space can be easily obtained as:

$$\begin{cases} \Delta\dot{x} = A\Delta x + B\Delta u \\ \Delta y = C\Delta x + D\Delta u \end{cases} \tag{36}$$

where Δx, Δu, and Δy represent state variables, input variables, and output variables, respectively; A is state matrix; and the dominant eigenvalues can be acquired by solving the roots of equation, i.e., $|sI\text{-}A|=0$, the amount of order of I is the same as that of A.

As for small-perturbation analysis, eigenvalue sensitivity is an important physical index, which can reflect the variation trend of the dominant eigenvalue in the system when a certain parameters change. If we define λ_i as the ith eigenvalue of eigenvalue matrix A, v_i^T and u_i are the left eigenvector and the right eigenvector of the eigenvalue λ_i, respectively. The eigenvalue sensitivity as for the parameter p can be derived as [15]:

$$\frac{\partial\lambda_i}{\partial p} = \frac{v_i^T \dfrac{\partial A}{\partial p} u_i}{v_i^T u_i} \tag{37}$$

where p means the any of system parameters. By means of eigenvalue sensitivity, the impact extent and tendency of a certain parameter on stability can be intuitively observed.

As shown in Table II, the eigenvalue sensitivity is obtained. The real and imaginary parts represent the influence of parameters on oscillation damping and frequency, respectively.

It indicates that the dark numbers mean that the eigenvalue is sensitive to the corresponding parameters. Clearly, virtual capacitance can increase damping and decline the oscillated frequency of dominant mode λ_5. However, virtual capacitance should be compromised for not too large, since the damping of λ_4 gets weaker as virtual capacitance increased. Virtual damping coefficient D_{dam} seems to contribute little to the critical eigenvalues. k_p is not beneficial to the damping of dominant eigenvalue λ_4. Other parameters impose little impact on eigenvalue sensitivity. It provides a guideline for control parameter design.

In actual, the denominator order of Z_{out} is one higher than numerator, which predominantly behaves like as capacitive. It would interact with DC network, which behaves as inductive if inappropriate control designed. Thus, the system can be simplified as a second-order one, shown as in Fig. 6.

In this case, to better match the power converter with DC network, virtual inertia control strategy should be designed and well-tuned with considering the whole system, Thus, simplified second-order system can be derived as:

$$H(s) = \frac{sL_{dc} + R_{dc}}{L_{dc}(C_{vir}+C)s^2 + (k_{dam}L_{dc} + R_{dc}(C_{vir}+C))s + R_{dc}k_{dam} + 1} \tag{38}$$

Since the standard second-order system can be expressed as:

$$\frac{\omega_n^{\,2}}{s^2 + 2\xi\omega_n s + \omega_n^{\,2}} \tag{39}$$

Hence, virtual inertia constant and virtual damping coefficient obeys the rules, i.e.,

$$\Rightarrow \begin{cases} \xi = \dfrac{k_{dam}L_{dc} + R_{dc}(C_{vir}+C)}{2\sqrt{L_{dc}(C_{vir}+C)(R_{dc}k_{dam}+1)}} \\ \omega_n = \sqrt{\dfrac{R_{dc}k_{dam}+1}{L_{dc}(C_{vir}+C)}} \end{cases} \tag{40}$$

where the above formula can provide a guideline for the design of k_{dam} and C_{vir}. Generally, to achieve a good damping performance and response, damping ratio ξ is normally designed as 0.707.

Besides, sensitivity as well as robustness performance proposed in Section IV-C can be referred to guide the control design as well.

F. Impedance analysis

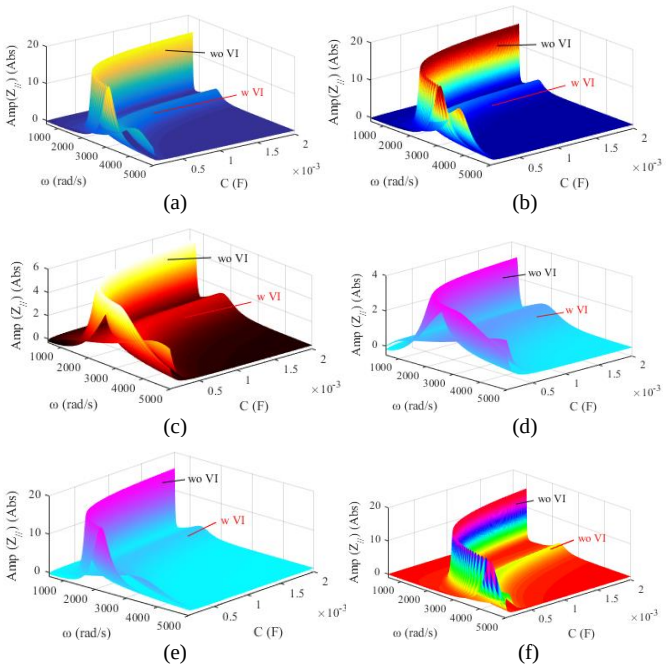

Fig. 19. 3-D frequency response characteristics of Z// with and without virtual inertia control strategy, (a) case 1, (b) case 2, (c) case 3, (d) case 4, (e) case 5, (f) case 6.

The specifications of system from Fig. 19(a) to Fig. 19(f) can be shown in Fig. 19. By means of changing the operation parameters of the system, frequency response characteristics of $Z_{//}$ are different. However, no matter how parameters vary, the resonance peaks are well damped with virtual inertia control strategy. It can be concluded that the proposed VI control

strategy can well dampen resonance peaks of the system, and thus mitigate oscillation of DC voltage and improve damping performance and stability for the system. As for all the figures, the resonance peaks are significantly declined with virtual inertia control strategy. As a result, the proposed VI control can improve damping performance of the system.

TABLE II EIGENVALUE SENSITIVITY ANALYSIS RESULTS

Eigenvalue / Parameters	λ_1	λ_2	λ_3	λ_4	λ_5
V_{dco}	-5.6e-5+3.4e-5j	5.57e-5+3.33e-5j	-8e-6	0.0101-0.0088j	0.0066+0.0057j
C_{vir}	0.0118-0.0129j	-0.0117-0.0128j	**3.8075**	**1.6356e3-1.4165e3j**	**-5.58e2-4.83e2j**
D_{dam}	0.0016-0.001j	-0.0016-0.001j	2.7055e-6	-0.1762+0.1526j	0.0089+0.0077j
k_{pv}	-0.0039+0.0023j	-0.0047-0.0028j	-3.654e-8	-0.0014+0.0001j	7.208e-5+6.56e-6j
k_{iv}	1.883e-4-3.048e-6j	-1.8e-4-2.913e-6j	5.185e-9	-1.327e-4-8.655e-6j	0.0131-0.0009j
k_{droop}	0.38	0.1524	-0.0113	-0.0234+0.0305j	-0.01-0.013j
k_{pi}	0.0017+0.0123j	-0.004-0.0188j	7e-6	**3.67-2.0304j**	0.14+0.0124j
k_{ii}	9.175e-6-1.346e-5j	1.132e-5+1.66e-5j	1.20e-8	-0.0157+0.009j	0.0062+0.0036j

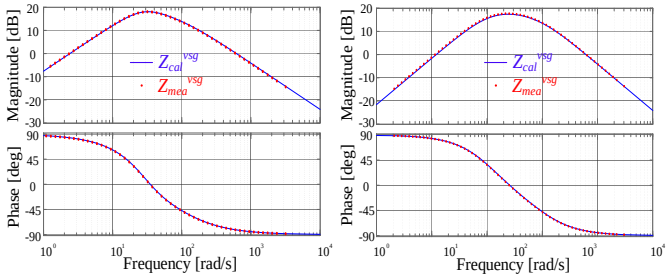

Fig. 20. Verification of the proposed modelling

To validate the effectiveness of proposed impedance model, a current injection is perturbed on the black box to acquire the corresponding voltage responses, which can be shown in Fig. 20. Clearly, the measured value matches well with the calculated model except for a tiny error in some frequencies, which well demonstrates the effectiveness of the proposed impedance model.

V. VALIDATIONS

A. *Simulations verification*

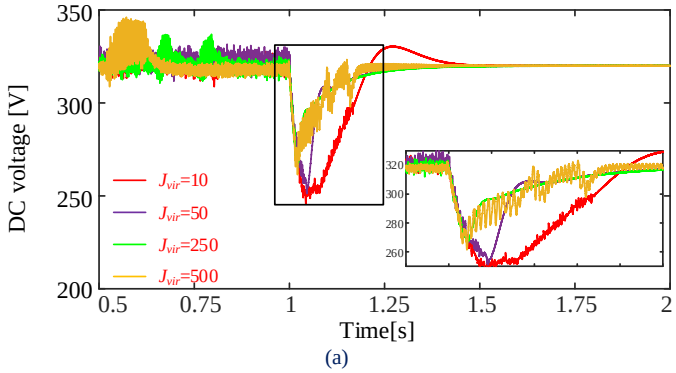

(a)

In this Section, the simulations platform based on a three DC converters as well as paralleled loads is developed to validate the effect of virtual inertia and virtual damping on the dynamics response of DC voltage during power disturbance. And the impact of various virtual inertia and virtual damping on DC voltage nadir (DCVN) and rate of change of DC voltage (RoCoV) are investigated comprehensively.

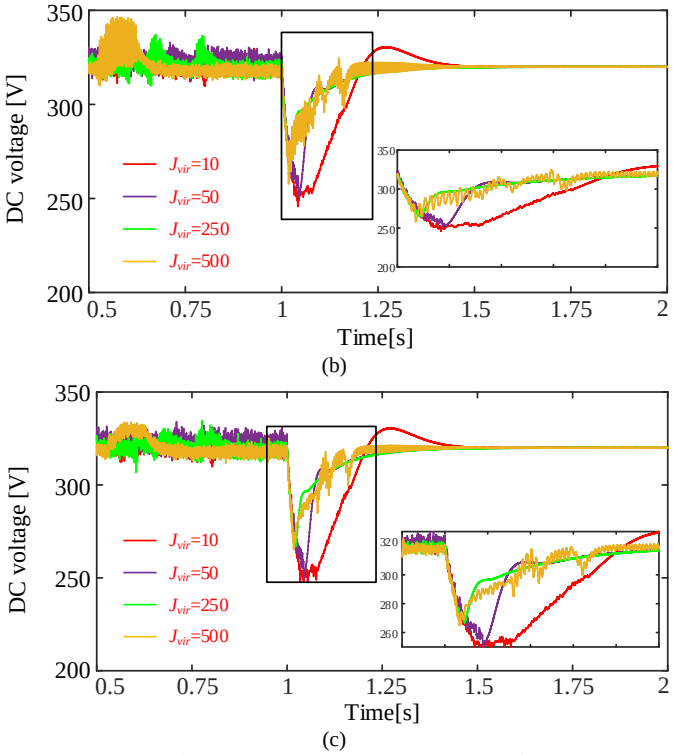

(b)

(c)

Fig. 21 The impact of various J_{vir} on the dynamic response of DC voltage with k_{dam}=3, and k_{virt}=10, (a) V_{dc1}, (b) V_{dc2}, (c) V_{dc3}

Fig. 21 shows the impact of various virtual inertia coefficients on DCVN and RoCoV when DC system is subjected to a step increment of active power with 10.24 kW.

Because the structure as well as the parameters of three DC converters are the same, the dynamics of DC voltage across the DC capacitor of three converters are almost the same during the power disturbance. Focused on Fig. 21(a), it can be seen that the larger virtual inertia coefficient J_{vir} leads to smaller DCVN and makes less transient DC voltage deviations, which is better for the stability and robustness performance when subjected to a power disturbance. It is because that larger virtual inertia makes the system response slower and thus the potential inertia from the source can supply larger inertia powers to compensate the power deficit, and thus the dynamic deviation is smaller as J_{vir} increased. From another view, as shown in Fig. 11, the virtual inertia control link is essentially an integral controller.

The larger J_{vir} brings stronger integral effect for the system, thus, DC voltage can track the reference DC voltage better and faster. Hence, DC voltage with larger J_{vir} seems to own stronger tracking capability with the reference DC voltage, i.e., 320 V in this paper.

In addition, it can be seen that larger VI J_{vir} returns DC voltage back to the initial nominal condition with a faster response. It is an indicator of better dynamic performance as well. From the energy conservation, smaller VI coefficient leads to larger DCVN and longer time to deviate the nominal voltage, which means that the larger VI can supply faster power support to the DC voltage restoration with a need for less energy. It can be inferred that the increased load powers provide larger inertial support for DC network, hence, the oscillation of DC voltage is dampened by the supplied inertia.

As a result, it can be inferred that larger virtual inertia is better for the stability and dynamic responses of the system and can supply larger inertial support, and can makes less voltage deviation and faster DC voltage restoration during the power disturbance.

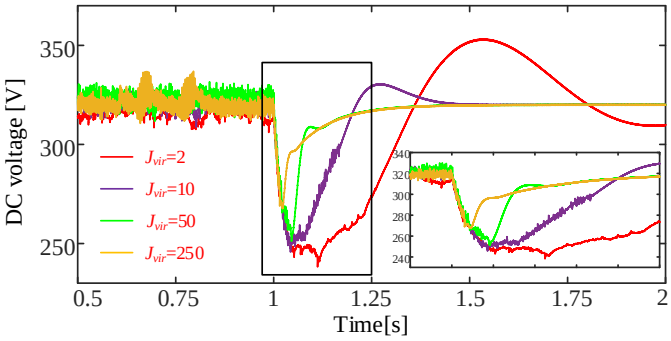

Fig. 22 The impact of various J_{vir} on the dynamic response of DC voltage with k_{dam}=3, and k_{virt}=10

It only displays one figure to show the dynamic response of DC voltage because the three voltages of different converters are nearly the same. It can be shown in Fig. 22, larger virtual inertia leads to less DCVN during the imbalanced powers. And larger virtual inertia constant lets DC voltage return back to the initially nominal value much faster. It can be concluded that the increase of J_{vir} is better for the stability of DC voltage during disturbance.

Besides, it can be clearly seen that oscillation appears before 1.0 s, and it is dampened by the proposed virtual inertia control strategy. Thus, virtual inertia has the capability to smooth the DC voltage and enhance the damping to suppress the oscillation of DC voltage.

Actually, no matter of Fig. 21 or Fig. 22, various J_{vir} leads to different RoCoV, but the effect is not so obvious. Besides, unlike the frequency, the requirement of RoCoV for DC voltage is not so important.

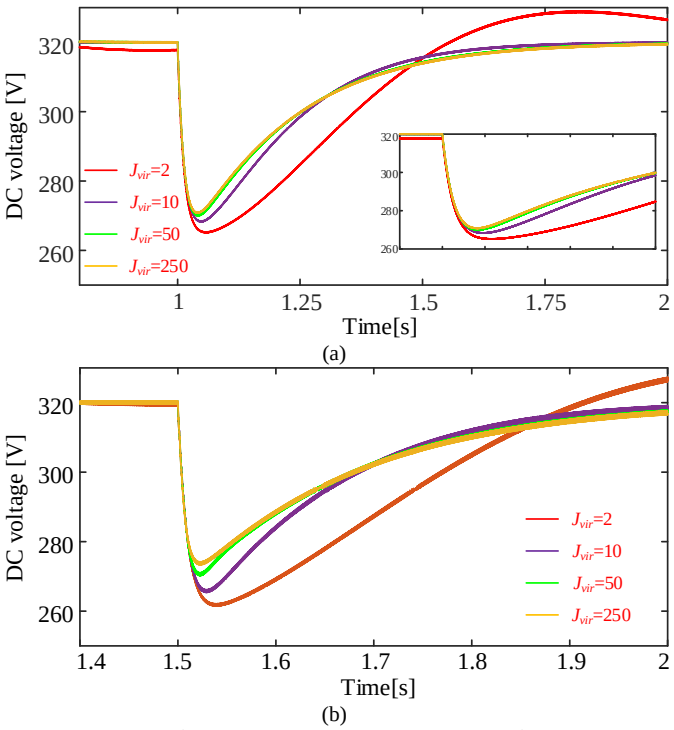

Fig. 23 The impact of various J_{vir} on the dynamic response of DC voltage with k_{dam}=3, (a) k_{virt}=20, (b) k_{virt}=15

To further investigate the impact of virtual resistance k_{virt} on the dynamic response of DC voltage. It can be found that the larger k_{virt} can lead to smaller dynamic deviation of DC voltage and less DCVN. Besides, it can help to mitigate the fluctuation of DC voltage, which indicates that larger k_{virt} contributes to enhancing damping of the system.

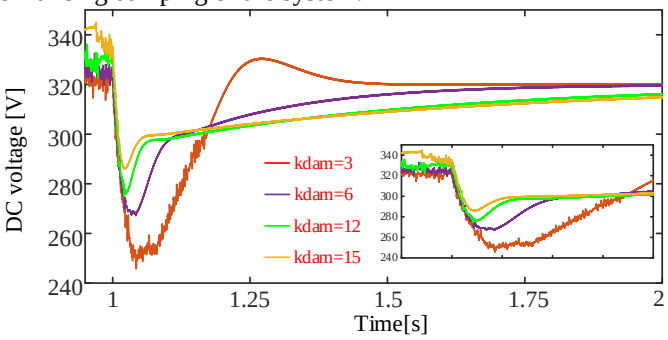

Fig. 24 The impact of various k_{dam} on the dynamic response of DC voltage with J_{vir}=10

Fig. 24 shows the impact of various virtual damping coefficient k_{dam} on the dynamic response of DC voltage. It is shown that the virtual damping can contribute to damping oscillation of DC voltage and enhance the transient response of DC voltage with smoother waveforms.

Moreover, larger k_{dam} results in less DCVN of DC voltage during disturbance. However, in the process of restoration of DC voltage, the conclusion is the inverse, i.e., larger k_{dam} means slower recovery of DC voltage, which is unfavorable for the restoration of DC voltage during disturbance.

Thus, the selection of k_{dam} should be compromised. Specifically, to acquire faster recovery response speed of DC voltage, k_{dam} should be as small as possible; while, to acquire less DCVN, k_{dam} should be as large as possible to guarantee the

DC voltage of the system deviate from the nominal value slower and less during the disturbance.

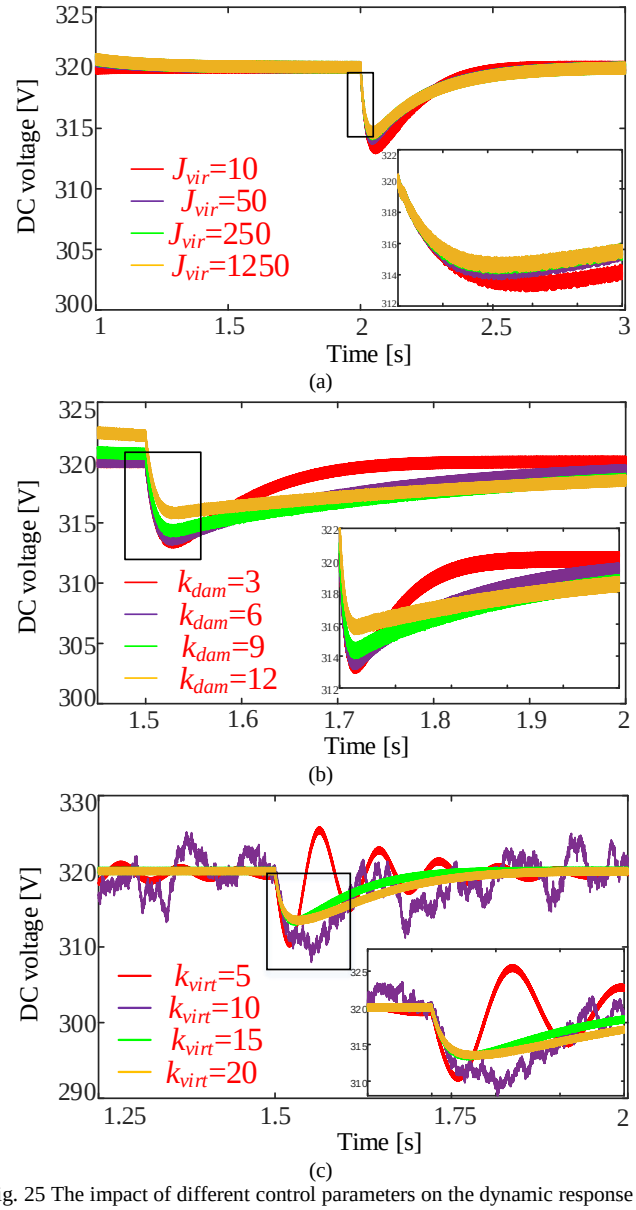

Fig. 25 The impact of different control parameters on the dynamic response of DC voltage with power increment of 1.024 kW, (a) variation of J_{vir} with k_{dam}=3 and k_{virt}=15, (b) variation of k_{dam} with J_{vir}=10 and k_{virt}=15, (c) variation of k_{virt} with J_{vir}=10 and k_{dam}=3

Fig. 25(a) shows the impact of various J_{vir} on the dynamic response of DC voltage when system is subjected to a power increment of 1.024 kW. In the process of DC voltage deviating from initial value, the greater virtual inertia leads to less DCVN, and the dynamic deviation of DC voltage is less. The speed of restoration of DC voltage is almost identical with different J_{vir}.

Fig. 25(b) displays the impact of various k_{dam} on the dynamic response of DC voltage, which shows that although greater virtual damping coefficient k_{dam} can lead to less DCVN during DC voltage deviating from the nominal value; but the greater k_{dam} results in much slower speed of restoration of DC voltage during restoration. k_{dam} is inversely proportional to the deviation of DC voltage, i.e., ΔV_{vir}, which indicates that during the deviation of DC voltage, the greater k_{dam} leads to less and slower deviation, while during the restoration, the greater k_{dam} results in less and slower deviation as well. Hence, it is controversial to select k_{dam} because the dynamic response in both deviation and restoration is much slower with greater k_{dam}. From another view, virtual damping coefficient contributes to impede the change of DC voltage, and thus the greater k_{dam} means stronger obstruction effect for DC voltage, i.e., DC voltage seems slower.

As shown in Fig. 25(c), the impact of various virtual resistance factor on the dynamic response of DC voltage during power increment is studied. It can be clearly seen that the attenuated oscillation of DC voltage occurs when k_{virt}=5 and k_{virt}=10. However, the DCVN gets less when k_{virt}=15 and k_{virt}=20. It illustrates that the increment of k_{vir} has the capability of suppressing oscillation of DC voltage and alleviating the deviation of DC voltage.

B. HIL experiments validation

To demonstrate the effectiveness of proposed theoretical analysis, the real-time semi-physical experimental platform is built. Fig. 26 shows the platform of RCP and HIL, which includes a host PC, a rapid control prototype, one hardware-in-the-loop platform, I/O board, and an oscilloscope. The experimental setup is constituted of two source-side DC boost converters, two CPL loads, and a grid-connected converter. It is noted that control parameters of dual-loop are the same for two DC converters.

Firstly, the abbreviations of "wVI" and "woVI" in Fig. 19 and from Fig. 27 to Fig. 29 represent the meaning of "with virtual inertia" and "without virtual inertia", respectively; hence wVI means with virtual inertia and woVI suggests without virtual inertia.

Fig. 27 shows the HIL experimental results of DC voltages across DC capacitance of boost converter. It should be remarkably noted that green curve denotes voltage of the 1st converter; purple curve represents voltage of 2nd converter.

It can be clearly seen from Fig. 27(a) that oscillation of DC voltages is well damped by the proposed virtual inertia control strategy. Thus, it can be concluded that virtual inertia control can mitigate oscillation caused by interaction between converter and DC lines, and provides a rough response, good damping performance, and enhanced stability margins for DC microgrid.

Compared to Fig. 27, parameters of the main circuit in Fig. 28 are invariable. However, the proportional and integral coefficient of outer voltage control loop is changed. DC voltages of the system fluctuate more largely than that of Fig. 27, when k_{pv} = 0.01, k_{iv} = 10 (Fig. 28(a)). Besides, the scope of fluctuation of DC voltage is smaller than that of Fig. 28(a), when k_{pv} = 0.5, k_{iv} = 100, k_{pi} = 5, k_{ii} = 100 (Fig. 28(b)). It can be observed that the oscillation of DC voltage has been well damped by the proposed virtual inertia control structure and has an exceedingly good dynamic performance with fast response. Hence, it can be inferred that the proposed virtual inertia control strategy can improve inertia and damping and thus make DC voltage change slower.

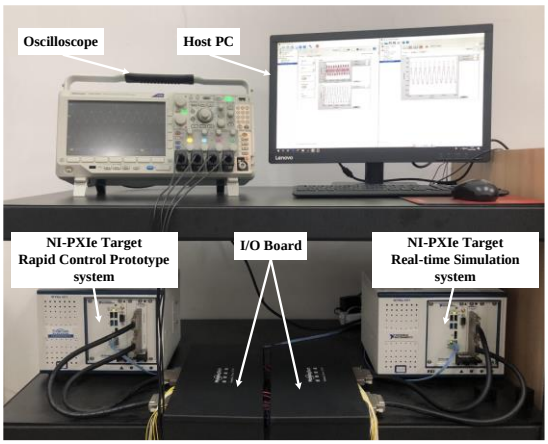

Fig. 26. Experimental platform

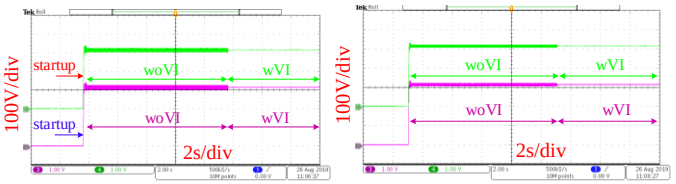

(a) (b)

Fig. 27. HIL experimental results of DC bus voltage of DC microgrid, (b) k_{pv} = 0.5, k_{iv} = 50, k_{pi} = 5, k_{ii} = 100, (b) k_{pv} = 0.01, k_{iv} = 50, k_{pi} = 5, k_{ii} = 100.

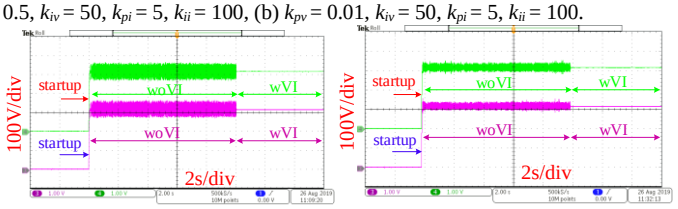

(a) (b)

Fig. 28. HIL results of DC bus voltage of DC microgrid, (a) k_{pv} = 0.01, k_{iv} = 10, k_{pi} = 5, k_{ii} = 100, (b) k_{pv} = 0.5, k_{iv} = 100, k_{pi} = 5, k_{ii} = 100.

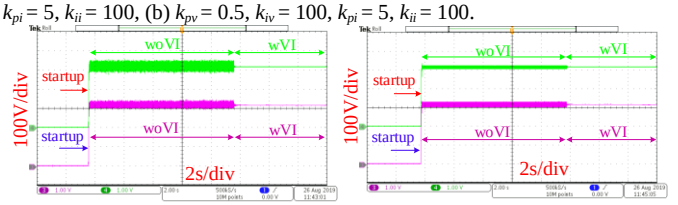

(a) (b)

Fig. 29. HIL results of DC bus voltage of DC microgrid, (a) k_{pv} = 0.1, k_{iv} = 30, k_{pi} = 5, k_{ii} = 100, (b) k_{pv} = 0.35, k_{iv} = 50, k_{pi} = 5, k_{ii} = 100.

Different from the above cases, we set two couples of specifications for the main circuit, i.e., R_1 = 0.1 Ω, R_2 = 0.4 Ω, L_1 = 12 mH, L_2 = 48 mH, R_{dc1} = 0.01 Ω, R_{dc2} = 0.03 Ω, L_{dc1} = 1 mH, L_{dc2} = 3 mH. Fig. 29(a) shows DC voltage of two DC converters with k_{pv} = 0.1, k_{iv} = 30, k_{pi} = 5, k_{ii} = 100. Clearly, even though PI control parameters of two converters are the same, scope of fluctuation of two DC voltages are different, because different main circuit parameters induce interaction of different extent. As shown in Fig. 29(b), DC voltage tends to be stable and has a rough response with the proposed virtual inertia control approach. It can be inferred that the virtual inertia control can dampen oscillation of DC voltage, enhance damping performance and inertia of the system, avoid adverse interaction, and improve stability of the system.

To validate the effectiveness of the current sharing mechanism, three DC boost converters feeding loads are built in Star-Sim HIL experimental setup. It should be noted that blue curve denotes 1st converter, the red curve refers to 2nd converter, and green curve represents 3rd converter.

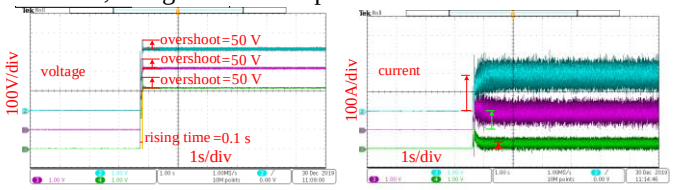

(a) (b)

Fig. 30. Validation of dynamic current sharing, (a) voltage, (b) current

As shown in Fig. 30, R_{dc1}=0.1 Ω, R_{dc2}=0.25 Ω, R_{dc3}=1 Ω, k_{droop1}=0.01, k_{droop2}=0.05, k_{droop3}=0.3. Clearly, the larger line resistance leads to larger current oscillation, and current sharing is inversely proportional to the sum of droops and line resistance, which means that larger droops and line resistance result in less average DC current sharing. The results well validate the current sharing theory. It can be seen that the overshoot of DC voltage of three converters are almost as the same as 50 V. It illustrates that the overshoot is mainly dependent on DC capacitance even though the line parameters are different. It also illustrates that the droop control gain and line parameters impose little effect on the overshoot of DC voltage. The rising time is as large as 0.1 s, which suggests that the system response is fast enough.

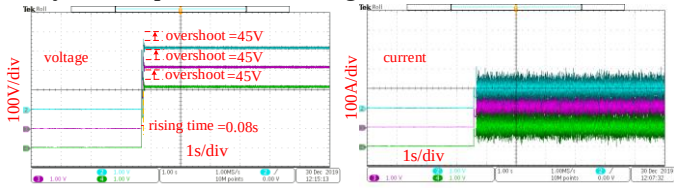

(a) (b)

Fig. 31. Verification of dynamic current sharing, (a) voltage, (b) current

As illustrated in Fig. 31, the dynamics of both voltages and currents resemble alike. It is because all of the parameters of three converters are the same. Thus, the current sharing is the same, and the dynamic current sharing is almost the same as well, which well demonstrates the current sharing mechanism.

It can be seen in Fig. 31 that the overshoot of DC voltage of three DC converters are almost as the same as 45 V, which suggests that the damping ratio is relative low. Besides, the rising time is about 0.08 s, which is much faster than that of Fig. 30, and it can be inferred that the damping ratio of DC voltage can be directly identified by the rising time and overshoot. It can be known that the overshoot of DC voltage can reflect the damping ratio of the system. Importantly, compared to Fig. 30, the overshoot is somewhat lower in Fig. 31. Hence, the oscillation amplitude of DC voltage in Fig. 31 is lower than that of Fig. 30, which illustrates that the damping ratios of the two cases are nearly the same.

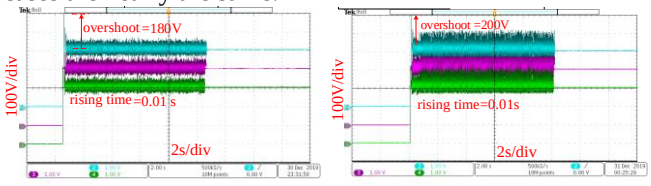

(a) (b)

Fig. 32. Impact of different sizes of virtual inertia capacitance, (a) C_{vir}=0.005 F, (b) C_{vir}=0.05 F

To further investigate the impact of virtual inertia on damping performance of the system, two different sizes of virtual capacitance are considered to dampen oscillation of DC

voltage, as shown in Fig. 32. Clearly, DC voltage oscillation can be well damped by two different sizes of virtual inertia constants. It well illustrates that the proposed cascaded virtual inertia control strategy radically improves the robustness regardless of size of virtual inertia. It also explains that the virtual inertia structure is robust enough. The results can also verify the eigenvalue analysis in Fig. 18(c) that the virtual inertia control strategy can radically suppress the oscillation of DC voltage and makes the dominant eigenvalues in the negative-real-axis to acquire the good damping performance. So, no matter of size of virtual inertia, the damping effect is good.

It can be clearly seen that in Fig. 32, because of different system parameters, the oscillation amplitude of DC voltage is much greater than that of Fig. 30 and Fig. 31. It illustrates that the damping ratio is much lower than that of Fig. 30 and Fig. 31. The rising time and overshoot of DC voltage also show that the damping ratio is much poorer than the former two cases. The shorter rising time and greater overshoot of DC voltage means the poorer damping, and leads to greater oscillation amplitude of DC voltage. Compared with Fig. 32(a) and (b), the overshoot of DC voltage in Fig. 32(b) is a little greater than that of Fig. 32(a), indicating the damping ratio of Fig. 32(b) is poorer than that of Fig. 32(a). Hence, the oscillation amplitude is a little greater as well.

Hence, the time-domain response of DC voltage can be effectively used to identify the oscillation amplitude of DC voltage, because the performance index can well reflect the damping ratio and response speed.

VI. Conclusions

This paper proposes a cascaded virtual inertia control strategy, which connects the voltage outer-loop and current inner-loop. The cascaded architecture of the proposed virtual inertia does not change the original control structure, improving the robustness of the control system a lot. Besides, a feedback-based analytical approach is originally proposed to identify the motion state of DC voltage, i.e., convergent or divergent oscillation, which is intuitive.

Dynamic current sharing mechanism is clearly clarified. We use the feedback concept to judge the motion state of DC voltage by means of vector diagram. Robustness analysis, eigenvalue analysis as well as eigenvalue sensitivity are developed to evaluate the dynamic characteristics, stability, robust stability, and robustness performance. It shows that the proposed cascaded virtual inertia control strategy has an extremely robust architecture, which enlarges the robustness of the system a lot. Eigenvalue shows that the proposed virtual inertia can make the dominant poles move along with negative axis, indicating the damping performance is enhanced a lot by the strategy. The parameters tuning is provided for the VSG control tuning. Impedance analysis is developed to intuitively observe the positive effect brought by the cascaded virtual inertia control scheme. The measured impedance model is well matched with the theoretical model. Finally, the theoretical analysis is validated by the HIL experiments.

The main contributions of this paper are organized as follows:

1) We propose a cascaded virtual inertia control strategy, connecting the voltage outer-loop and current inner-loop, which do not change the original control structure and keep a certain robustness of the control structure.

2) We propose a feedback analytical approach to more intuitively identify the motion state of DC voltage, which helps us more deeply comprehend the stability and dynamics of DC voltage. The approach can be extended to other power electronics systems.

3) It is found that the proposed virtual inertia control can improve inertia as well as damping of the system a lot. Robustness as well as robust stability is enhanced a lot.

4) Besides of the above advantages of the proposed cascaded virtual inertia control strategy, it is found that the proposed cascaded virtual inertia control strategy can lessen DCVN in the transient after disturbance, and can lead to faster restoration of DC voltage and thus make DC voltage return back to the initial DC voltage faster. That is to say, the proposed virtual inertia control can not only dampen oscillation caused by interactions, but also improve the damping performance and transient response due to the imbalanced powers.

Appendix

$$V_{re} = (V_{dc0} + k_{vir} I_{vir0})$$

$$kdam = -(\frac{V_{dc0} I_{vir0}}{\omega_{vir0} f_{yT} Q} + I_{vir0} - \frac{\omega_{vir0} D_{dam}}{f_{yT} Q})$$

$$Z_{dcnet} = \frac{(R + R_{CPL}) + sL}{LCs^2 + (R + R_{CPL})Cs + 1}$$

References

[1] Zhu. J, B. CD, A. GP, Roscoe AJ, Bright CG, "Inertia emulation control strategy for VSC-HVDC transmission systems", *IEEE Trans Power. Syst*., vol. 28, no. 2, pp. 1277-1287, May. 2013.

[2] B. FD, D. JL. "Coordinated frequency control using MT-HVDC grids with wind power plants", *IEEE Trans Sustain. Energy*., vol. 7, no. 1, pp. 213-220, Jan. 2016.

[3] T. P, V. Hertem D. The relevance of inertia in power systems. Renew Sustain Energy Rev 2016; 55: 999-1009.

[4] N. Rashidirad, M. Hamzeh, K. Sheshyekani, and E. Afjei, "A simplified equivalent model for the analysis of low-frequency stability of multi-bus DC microgrids", *IEEE Trans. Smart. Grid*., DOI.10.1109/TSG.2017.2705194

[5] Y. Song, and F. Blaabjerg, "Wide frequency band active damping strategy for DFIG system high frequency resonance", *IEEE Trans. Energy. Convers*., vol. 31, no. 4, pp. 1665-1675, Dec. 2016.

[6] N. Rashidirad, M. Hamzeh, K. Sheshyekani, and E. Afjei, "An effective method for low-frequency oscillations damping in multibus DC microgrids", *IEEE J. Emerg. Sel. Topic Circuit Syst*., vol. 7, no. 3, pp. 403-412, Sep. 2017.

[7] M. Amin, and M. Molinas, "Understanding the origin of oscillatory phenomena observed between wind farms and HVDC systems", *IEEE J. Emerg. Sel. Topics Power Electron*., vol. 5, no. 1, pp. 378-392, Mar. 2017.

[8] M. Lu, X. Wang, P. C. Loh, and F. Blaabjerg, "Resonance interaction of multiparallel grid-connected inverters with LCL filter", *IEEE Trans. Power. Electronics*., vol. 32, no. 2, pp. 894-899, Feb. 2017.

[9] S. S, M. K. Damping of Subsynchronous Oscillations By an HVDC Link. An HVDC Simulator Study. *IEEE Trans Power App Syst* (through 1985) 1981; PAS-100(3): 1431-39.

[10] X. Lu, K. Sun, J. M. Guerrero, J. C. Vasquez, L. Huang, and J. Wang, "Stability enhancement based on virtual impedance for DC microgrids with constant power loads", *IEEE Trans. Smart Grid*., vol. 6, no. 6, pp. 2770-2783, Nov. 2015.

[11] N. Rashidirad, M. Hamzeh, K. Sheshyekani, and E. Afjei,

"High-frequency oscillations and their leading causes in DC microgrids", *IEEE Trans. Energy conversion*., vol. 32, no. 4, pp. 1479-1491, Dec. 2017.

[12] L. Xu, L. Fan, and Z. Miao, "DC impedance-model-based resonance analysis of a VSC-HVDC system", *IEEE Trans. Power Del*., vol. 30, no. 3, pp. 1221-1230, Jun. 2015.

[13] G. Pinares, and M. Bongiorno, "Analysis and mitigation of instabilities originated from DC-side resonances in VSC-HVDC systems", *IEEE Trans. Ind. Appl*., vol. 52, no. 4, pp. 2807-2815, Jul. 2016.

[14] G. Pinares, and M. Bongiorno, "Modeling and Analysis of VSC-Based HVDC systems for DC network stability studies", *IEEE Trans. Power. Del*., vol. 31, no. 2, pp. 848-856, Apr. 2016.

[15] L. Guo, S. Zhang, X. Li, Y. Li, C. Wang, and Y. Feng, "Stability analysis and damping enhancement based on frequency-dependent virtual impedance for DC microgrid", *IEEE J. Emerg. Sel. Topics Power Electron*., vol. 5, no. 1, pp. 338-350, Mar. 2017.

[16] X. Zhang, Q. Zhong, V. Kadirkamanathan, J. He and J. Huang, "Source-Side Series-Virtual-Impedance Control to Improve the Cascaded System Stability and the Dynamic Performance of Its Source Converter," in *IEEE Transactions on Power Electronics*, vol. 34, no. 6, pp. 5854-5866, June 2019.

[17] W. Wang, M. Barnes, O. Marjanovic, and O. Cwikowski, "Impact of DC breaker systems on multiterminal VSC-HVDC stability", *IEEE Trans. Power. Del*., vol. 31, no. 2, pp. 769-779, Apr. 2016.

[18] A. Kwasinski, and C. Onwuchekwa, "Dynamic behavior and stabilization of DC microgrids with instantaneous constant-power loads," *IEEE Trans. Power Electron*., vol. 26, no. 3, pp. 822–833, Mar. 2011.

[19] X. Lu, K. Sun, J. M. Guerrero, J. C. Vasquez, L. Huang, and J. Wang, "Stability enhancement based on virtual impedance for DC microgrids with constant power loads", *IEEE Trans. Smart. Grid*., vol. 6, no. 6, pp. 2770-2783, Nov. 2015.

[20] A. Riccobono, and E. Santi, "Comprehensive review of stability criteria for DC power distribution systems", *IEEE Trans. Ind. Appl*., vol. 50, no. 5, pp. 3525-3535, Sep. 2014.

[21] E. Unamuno and J. Barrena, "Equivalence of primary control strategies for AC and DC microgrids," Energies, vol. 10, no. 12, p. 91, Jan. 2017.

[22] C. Li, Y. Li, Y. Cao, H. Zhu, C. Rehtanz and U. Häger, "Virtual Synchronous Generator Control for Damping DC-Side Resonance of VSC-MTDC System," in *IEEE Journal of Emerging and Selected Topics in Power Electronics*, vol. 6, no. 3, pp. 1054-1064, Sept. 2018.

[23] K. Rouzbehi, J. I. Candela, G. B. Gharehpetian, L. Harnefors, A. Luna, and P. Rodriguez, "Multiterminal DC grids: Operating analogies to AC power systems," Renew. Sustain. Energy Rev., vol. 70, pp. 886–895, Apr. 2017.

[24] Y. Hirase, K. Sugimoto, K. Sakimoto, and T. Ise, "Analysis of resonance in microgrids and effects of system frequency stabilization using a virtual synchronous generator", *IEEE J. Emerg. Sel. Topics Power Electron*., vol. 4, no. 4, pp. 1287-1298, Dec. 2016.

[25] M. A. Torres L., L. A. C. Lopes, L. A. Mor án T., and Jos é R. Espinoza C., "Self-tuning VIRTUAL INERTIA: A control strategy for energy storage systems to support dynamic frequency control", *IEEE Trans. Energy conversion*., vol. 29, no. 4, pp. 833-840, Dec. 2014.

[26] J. Liu, Y. Miura, and T. Ise, "Comparison of dynamic characteristics between virtual synchronous generator and droop control in inverter-based distributed generators", *IEEE Trans. Power Electron*., vol. 31, no. 5, pp. 3600-3611, May. 2016.

[27] M. Guan, W. Pan, J. Zhang, Q. Hao, J. Cheng, and X. Zheng, "Synchronous generator emulation control strategy for voltage source converter (VSC) stations", *IEEE Trans. Power Syst*., vol. 30, no. 6, pp. 3093-3101, Nov. 2015.

[28] H. Wu, X. Ruan, D. Yang, X. Chen, W. Zhao, Z. Lv, and Q. Zhong, "Small-signal modeling and parameters design for virtual synchronous generators", *IEEE Trans. Ind. Electron*., vol. 63, no. 7, pp. 4292-4303, Jul. 2016.